Applications of Miniaturized Ultrasound Powered Wireless

Nerve Stimulators for Pain Management

by

Xi Zong

A Thesis Presented in Partial Fulfillment
of the Requirements for the Degree
Master of Science

Approved November 2014 by the
Graduate Supervisory Committee:

Bruce Towe, Chair
Jeffrey Kleim
Marco Santello

ARIZONA STATE UNIVERSITY

December 2014

ABSTRACT

Peripheral Vascular Disease (PVD) is a debilitating chronic disease of the lower extremities particularly affecting older adults and diabetics. It results in reduction of the blood flow to peripheral tissue and sometimes causing tissue damage such that PVD patients suffer from pain in the lower legs, thigh and buttocks after activities. Electrical neurostimulation based on the "Gate Theory of Pain" is a known to way to reduce pain but current devices to do this are bulky and not well suited to implantation in peripheral tissues. There is also an increased risk associated with surgery which limits the use of these devices. This research has designed and constructed wireless ultrasound powered microstimulators that are much smaller and injectable and so involve less implantation trauma. These devices are small enough to fit through an 18 gauge syringe needle increasing their potential for clinical use. These piezoelectric microdevices convert mechanical energy into electrical energy that then is used to block pain. The design and performance of these miniaturized devices was modeled by computer while constructed devices were evaluated in animal experiments. The devices are capable of producing 500ms pulses with an intensity of 2 mA into a 2 kilo-ohms load. Using the rat as an animal model, a series of experiments were conducted to evaluate the in-vivo performance of the devices.

DEDICATION

Every challenge needs the self effort as well as guidance from those who were so close to my heart. I would like to dedicate my humble effort to my sweet and loving

Mentor: Dr.Bruce Towe

Lin Sun

Father: Mr. Yong Zong

Mother: Ms. NanNan Xie

whose affection, love and encourage allow me to complete my graduate study and overcome every challenge in my life.

ACKNOWLEDGMENTS

TABLE OF CONTENTS

LIST OF TABLES

LIST OF FIGURES

Figure   Page

CHAPTER 1

INTRODUCTION

Peripheral Vascular disease

Peripheral vascular disease (PVD), also known as peripheral artery disease, is a condition that develops when the arteries that supply blood to the internal organs, arms, and legs become completely or partially blocked as a result of atherosclerosis. PVD of lower extremities can be a source of intense pain of lower legs, thigh and buttocks.   Pain is often triggered by such as only a short distance of walking.

According to the Centers for Disease Control and Prevention, approximately 8 million people in the United States alone have peripheral vascular disease, which includes 12-20% of the population above 60 years of age. Although not all individuals who are diagnosed with PVD experience leg pain, it is estimated that 60% or more of the patients diagnosed with PVD experience some leg pain [1].

Treatment may slow or stop disease progress and reduce the risk of complications. Without treatment, PVD can cause sores or gangrene (tissue death). In extreme cases, it may be necessary to remove part of the leg or foot (amputation).

Treatments for peripheral vascular disease include lifestyle changes, medicines, and surgery or procedures. The overall goals of treating PVD include reducing symptoms, improving quality of life, and preventing complications. Treatment is based on the signs and symptoms, risk factors, and results from a physical exam and tests.

CHAPTER 2

BACKGROUND

Nerve Stimulation

Nerve stimulation is an important clinical therapeutic technique used to treat chronic neurological diseases and relieve pain. In 46 AD, Scribonius Largus used torpedo fish (electric ray) to relieve headaches. This experiment is the first recorded use of neural stimulation [2]. Later in 18th century, Luigi Galvani discovered that the muscles of dead frog legs twitched when struck by direct current on the nervous system [3]. In modern times, neural stimulation is used in devices such as visual implants, cochlear implants, spinal cord stimulators, and deep brain stimulation implants.   These devices employ small electrical currents that can cause bioelectrical action events in a nerve, muscle, and brain and so induce functionality in the nervous system.

Peripheral nerve stimulation (PNS) places electrodes along the course of a peripheral nerve and drives currents for testing neural muscle conduction in anesthesia; autonomic stimulation for treatment of urinary and gastrointestinal disorders; and for control of Parkinson's symptoms. PNS presents an excellent modality to treat neuropathic pain [4] and complements other electrical stimulation therapies such as spinal cord stimulation (SCS) and deep brain stimulation (DBS). In terms of approved indications, SCS is more widely used than PNS; however, the interest on PNS has been increasing over the recent years because of its less invasive characteristic.

Although deep brain stimulation and spinal cord stimulation has been relatively well developed, they are still limited by a bulky size, invasiveness, and riskiness of the surgical procedure. Both of the procedures have been known to cause further complications as a result of their stimulation function as well as the potential for infection and issues relative to the placement of the electrode system in the sensitive spinal lumen. These factors are the biggest concerns in the SCS and DBS. A type of neural stimulator investigated in this thesis targets pain relief caused by PVD. It employs the same bioelectrical mechanism as DBS and SCS.

Gate Theory of Pain Inhibition

Pain is defined by the International Association for the Study of Pain as an unpleasant sensory and emotional experience associated with actual or potential tissue damage, and described in terms of such damage.

Pain is always subjective. Each individual learns the application of the word through experiences related to injury in early life. Biologists recognize that those stimuli which cause pain to be liable to damaged tissue. Accordingly, pain is experience that we associate with actual or potential tissue damage. It is unquestionably a sensation in a part or parts of the body, but it is also always unpleasant and therefore also an emotional experience.

Pain can be classified based on pain physiology, intensity, temporal characteristics, type of tissue affected, and syndrome as follows:

- Pain physiology (nociceptive, neuropathic, inflammatory)
- Intensity (mild-moderate-severe; 0-10 numeric pain rating scale)
- Time course (acute, chronic)
- Type of tissue involved (skin, muscles, viscera, joints, tendons, bones)
- Syndromes (cancer, fibromyalgia, migraine, others)

There are two major afferent pain sensation neurons, C fibers and A delta(Aδ) fiber. C fibers are one of the classes of nerve fiber in the central nervous system and peripheral nervous system. The C group fibers are unmyelinated and have a small diameter and low conduction velocity. They respond to stimuli such as cold and pressure, and, as nociceptors,; that is, stimulation of them is interpreted as fast/first pain information. Because A delta fibers are thinly myelinated, they send impulses faster than unmyelinated C fibers.

It was suggested that C fibers are predominantly response to chronic pain and A delta fiber are predominantly response to acute pain. The large fibers carry touch and pressure as well as joint position sense. These fibers are myelinated, hence faster in conducting impulses from the periphery to the brain. Small nerve fibers (pain receptors) and large nerve fibers ("normal" receptors) synapse on projection cells (P), which go up the spinothalamic tract to the brain, and

3

inhibitory interneurons (I) within the dorsal horn [5]. It was suggested that in the central nerve system (CNS), there is a circuit which can modulate incoming pain information. The first pain modulation mechanism, the "Gate Control" theory was proposed by Melzack and Wall in the mid 1960s [6]. The concept of the gate control theory is that non-painful input closes the gates to painful input, which results in prevention of the pain sensation from traveling to CNS.
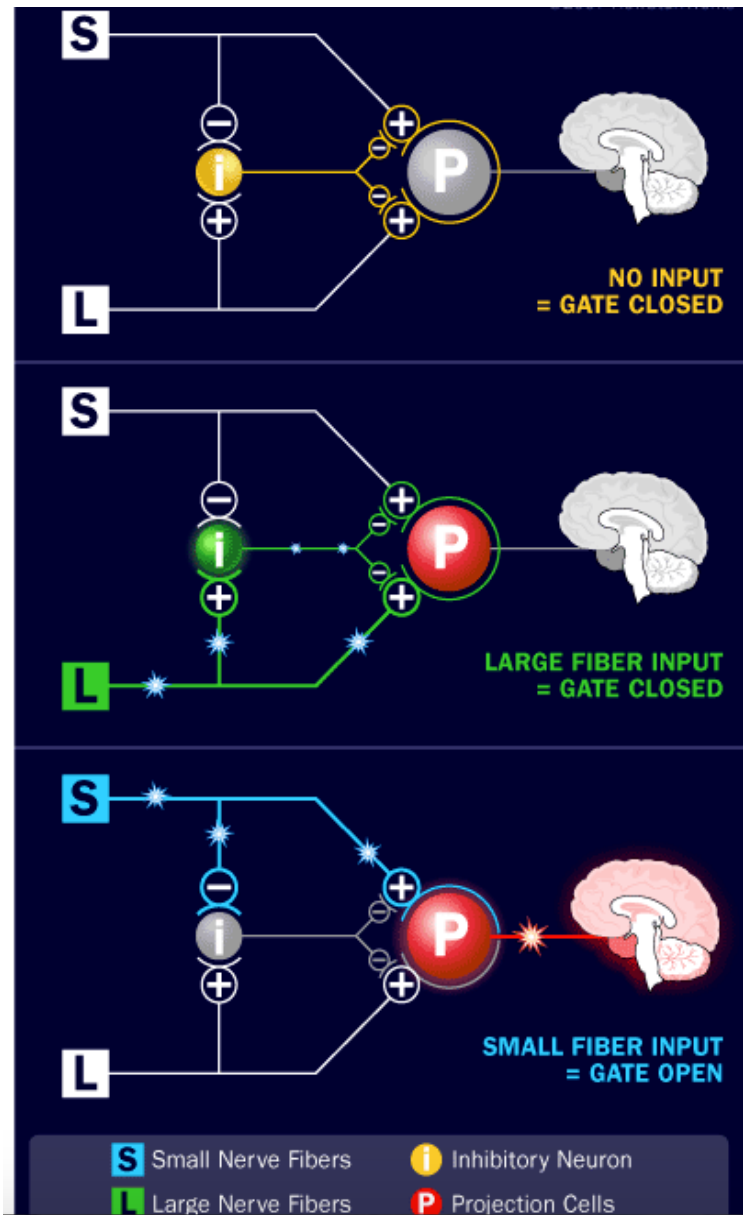
Figure 1 Gate Theory of Pain

Figure 1 illustrates the three situations in gate control theory [5].

1. When no input comes in, the inhibitory neuron prevents the projection neuron from sending signals to the brain (gate is closed).

2. Normal somatosensory input happens when there is more large-fiber stimulation (or only large-fiber stimulation). Both the inhibitory neuron and the projection neuron are stimulated, but the inhibitory neuron prevents the projection neuron from sending pain signals to the brain (gate is closed).

3. Nociception (pain reception) happens when there is more small-fiber stimulation or only small-fiber stimulation. This inactivates the inhibitory neuron, and the projection neuron sends signals to the brain informing it of pain (gate is open).

A study shows that prolonged, low-frequency activation of high-threshold, and primary afferents can activate inhibitory mechanisms in the central nervous system (CNS) which attenuate the activity of nociceptive pathways mediating the tail withdrawal reflex. This inhibition can be elicited by stimulation of local or more remote peripheral sites [7].

Piezoelectric Effect for Transferring Energy to Biomedical Implants

Traditional methods of neurostimulation use an implantable pulse generator with an on-board battery that is rechargeable. When the battery is ultimately depleted, usually after five to six years, the implant generally needs to be surgically explanted and replaced. This technique requires repeated invasive surgeries, a risk of infection, and a possibility of lead breakage [8].

During the last few decades, researchers have investigated powering a wireless device with ultrasound energy [9] [10] [11] [12] [13]. In 2011, Larson and Towe successfully used a cylindrical PZT-5A element of 1.13 mm diameter, 1 mm thick (giving a volume of 1 mm3) to power a biomedical implant and achieved motor stimulation in rat [14]. Such designs are wireless, miniaturized, implantable devices. The integration of piezoelectric component makes the device battery-free.

In this work, a piezoelectric material acts as the power supply for the stimulator where its generated energy is converted directly to a stimulation pulse without an intervening electronics. The stimulation pulse characteristics, namely the pattern of pulse frequency, intensity and pulse duration, are controlled by the envelope of applied ultrasound. In this configuration, the ultrasound is applied externally, resulting in more freedom in pulse wave shape than implanted pulse generators that are hardwired or permanently coded with pulse shapes.

Although the distance between the neural stimulator and the ultrasound traducer is only a few centimeters, this few centimeters crosses the border of internal environment with the external environment. By using ultrasound and piezoelectric components, this study has successfully made a wireless power connection between internal and external environments.

Piezoelectric Effect in Matter

The piezoelectric effect was discovered in 1880 by the bothers Pierre Curie and Jacques Curie. It is the production of an electric field by applying a mechanical stress to an ordered crystalline material (called the generator mode); and the converse effect where stress is produced within the piezoelectric material as a result of an applied potential difference (motor mode).

When sound energy interacts with PZT material, it can be harvested as an electrical energy source. Piezoelectric materials can be divided in two main groups: crystals and ceramics. Some of the mostly commonly known piezoelectric material includes: Quartz (SiO_2), Tourmaline, Barium titanate ($BaTiO_3$), Lead zirconate titanate (PZT), and Polyvinylidene fluoride (PVDF). Of this group, PZT and PVDF are most commonly used because they have relatively higher outputs than quartz. In the proposed application, this study focus on using ultrasound to drive PZT to generate charge for electrical neural stimulation.

The piezoelectric material quality is the most important in design of devices based on piezoelectricity. The conversion efficiency from mechanical energy of an ultrasound wave to electrical energy can be as high as 10%.

Piezoelectric Material Performance

Synthetic piezoelectric materials such as PZT exhibit electrical polarization in a single direction that results from a poling process applied to ceramic material in their manufacture. Piezoelectrics are made from non-poled ceramics by applying electrical field above their curing temperature. They are sensitive to the vector direction of the force applied on them. It is this vector sensitivity of PZT material to acoustic forces that must be taken into account in a piezoelectric conversion device for biomedical application. Based on how the piezoelectric material is cut and how the external forces are applied relative to the poling direction, the piezoelectric element exhibits three main modes of generation: transverse, longitudinal, and shear.

The strength of the generated electric field depends on the following factors: the properties of the piezoelectric element, the size and shape of the element, the directions of the applied forces and the electrical excitation. To give a more clear introduction about this theory, three axis are used to identify the directions in a piezoelectric element, named as 1, 2, 3, which are analogous to X, Y, Z of the typical dimensional orthogonal set of axes [15].

As shown in figure 6, the axis labeled as 3 is parallel to the direction of the ceramic polarization direction. This direction is established by a high DC voltage that is applied between a pair of conductively coated surfaces that provide poling during manufacturing. "P" is the polarization vector pointing from the positive to the negative polling electrode.

G constant is the piezoelectric constant representing the relationship between the electric field produced by a mechanical stress. It is expressed as the equation of

$$g = \frac{\text{open circuit electric field}}{\text{applied mechanical stress}}$$

The unit of this equation is volts/meter per newton/square meter.

The output voltage can be obtained by multiplying the electrical field and the thickness of the ceramic between its two coated surfaces. Different subscripts indicate the relationship between the electric field and the mechanical stress applied on the piezoelectric element [16].

A "33" subscript indicates that the electric field and the mechanical stress are both along the polarization axis (Figure 3). A "31" subscript signifies that the pressure is applied at right angles to the polarization axis, but the voltage appears on the same electrodes as in the "33" case. (Figure 4). A "15" subscript implies that the applied stress is shear and that the resulting electric field is perpendicular to the polarization axis (Figure 5).
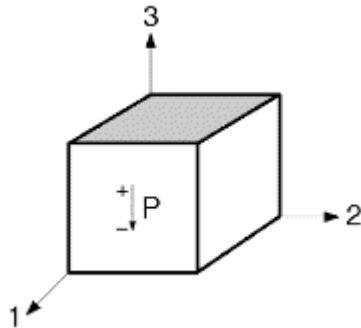
Figure 2 The Axis of the Piezoelectric Element
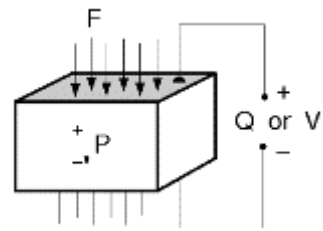
Figure 3 Longitudinal Mode: A "33" Subscript
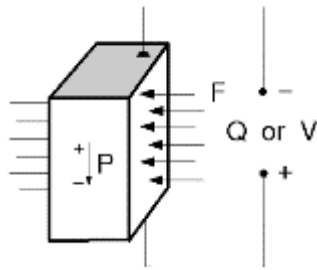
Figure 4 Transverse Mode: A "31" Subscript.
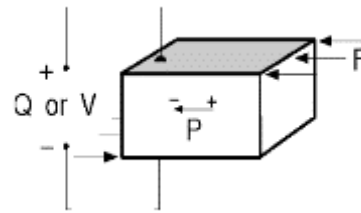
Figure 5 Sheer Mode: A "15" Subscript.

High g_{ij} constants favor large voltage output, and are sought after for sensors. Although the g coefficient are called voltage coefficients, it is also correct to say the g_{ij} is the ratio of strain developed over the applied charge density with units of meters per meter over coulombs per square meter.

As mentioned, PZT has different operation mode. How much current it can generate depends on the size of the piece of the PZT, the force applied on it and the g constant.

These factors are important in the design of miniature implanted biomedical devices powered by ultrasound transferring energy to a piezoelectric material. The size of the PZT element

is constrained by the desire to be small and the dimensions of the packaging polyimide tube. For efficient operation, it is crucial to increase the current generated; that is, the bigger g constant the better. Table 1 is the PZT-5A material properties from Piezo System, inc.

PIEZOELECTRIC & MATERIAL PROPERTIES OF PSI-5A4E SINGLE SHEETS

PIEZOELECTRIC

Composition		Lead Zirconate Titanate	
Piezo Systems Material Designation		Type 5A4E (Industry Type 5A, Navy Type II)	
Relative Dielectric Constant (@1KHz)	K^T_3	1800	
Piezoelectric Strain Coefficient	d_{33}	390×10^{-12}	meter/Volt
	d_{31}	-190×10^{-12}	meter/Volt
Piezoelectric Voltage Coefficient	g_{33}	24.0×10^{-3}	Volt meter/Newton
	g_{31}	-11.6×10^{-3}	Volt meter/Newton
Coupling Coefficient	k_{33}	0.72	
	k_{31}	0.35	
Polarization Field	Ep	2×10^6	Volt/meter
Initial Depolarization Field	Ec	5×10^5	Volt/meter

MECHANICAL

Density	ρ	7800	Kg/meter^3
Mechanical Q		80	
Elastic Modulus	Y^E_3	5.2×10^{10}	Newton/meter^2
	Y^E_1	6.6×10^{10}	Newton/meter^2

THERMAL

Thermal Expansion Coefficient		$\sim4 \times 10^{-6}$	meter/meter °C
Curie Temperature		350	°C

Table 1 Piezoelectric Material Properties of PZT 5-A

Thus the vector direction of the applied ultrasound force is important relative to the piezoelectric position and orientation. When PZT is driven by ultrasound in g_{33} mode, the force applied direction and the charge generating directions are parallel, the voltage outputs are highest. However, the disadvantage of g_{33} mode is that the angular sensitivity is increased. The reason will be explained in detail in the result sections of this chapter.

Equivalent Circuit

A piezoelectric generator has high DC output port impedance and can be modeled as voltage source. The voltage at the source is related to the applied forces and the property of the piezoelectric element [18].
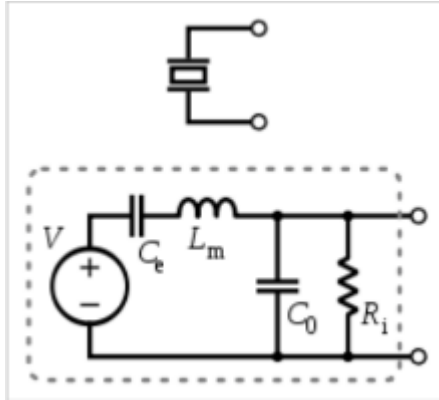
Figure 6 Piezoelectric Equivalent Circuit.

In 2000, Alfredo Vázquez Carazo came up with the detailed model with the effects of the sensor's mechanical construction and other non-idealities [19]. As shown in figure 5, Lm represents the seismic mass and inertia of the sensor itself. Ce is inversely proportional to the mechanical elasticity of the sensor. C0 represents the static capacitance of the transducer resulting from an inertial mass of infinite size. Ri is the insulation leakage resistance of the transducer element [19]. Since Ri is very large compare to the equivalent impedance of C0, C0 become dominant in this case. In some cases when we are measuring the electrode impedance, we only consider about the effect of the capacitor. As we see from the equation,:

$$Z_C = \frac{1}{j\omega C}$$

the equivalent impedance of the capacitor is highly depend on the frequency, in our case, is the frequency of the external applied ultrasound.

Ultrasound Properties

Ultrasound is a high frequency mechanical wave transferred by compression and rarefaction of matter. As a wave in matter, it carries kinetic energy that at high frequency can be focused and directed to a beam. The energy density carried by ultrasound is relatively higher compared to the energy density carried by electrical wave.

The use of ultrasound for energy transfer in biomedical applications is increasingly recognized because the high energy density is achievable with essentially no biological effect. Furthermore, the higher efficiency of the energy transfer allows conservation battery life on the external driver unit.

As the frequency goes up the energy carried by the wave is greater and the other properties of the beam such as the ability to focus is improved. Hence it is desirable to use higher frequency to transfer energy to body tissue. However, the attenuation of the ultrasound in tissue increases as the frequency goes up as seen in the following equations.

$$I(z) = I_0 e^{-\alpha z}$$

$$\text{Attenuation} = \alpha[dB/(MHz \cdot cm)] \cdot \ell[cm] \cdot f[MHz]$$

Therefore, there is a trade off in medical ultrasound whereby the frequency that is chosen is a compromise between tissue penetration and energy density in transfer in the beam. Ozeri et al. (2011) suggest the use of ultrasound energy for example in recharging implantable battery for the electrical devices implanted in body [9]. However, there is no reported pure ultrasound powered implantable devices in scientific literature.

PZT Actuated by Ultrasound

Sound is a mechanical wave that propagates through a material medium. The mechanical wave itself results from the vibration of the particles of the medium. If a sound wave is moving from left to right through water, when the energy of the sound is passing through it, the water particle will be displaced left and right. If it is considered as longitudinal waves, the motion of the particles is parallel to the direction of the sound propagation.

When the PZT is placed in the path of ultrasound, it will experience the pressure-rarefaction force of the sound wave. The sign of the electrical charge generation corresponds to the direction of the force. Figure 7 shows the charge generation in a rectangle of PZT aligned with the ultrasound wave path. The voltage generated along the length alternates with the pressure. Figure 5 shows the AC output of the piezoelectric transducer excited using an ultrasound transducer at one slice through the PZT from top to bottom. However, if the PZT generated electrodes are located at the top and bottom, then there may be diminishment or even cancellation of charge generation by the shorting effect of the electrodes. This means that care must be exercised in the design of the piezoelectric ultrasound receiver's size and shape, selection of operating frequency, and its mode of operation.
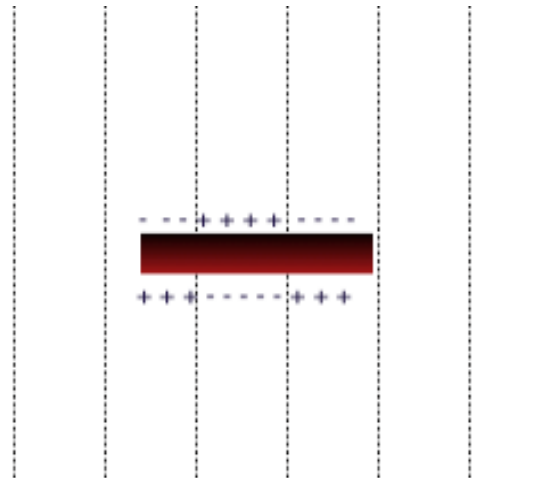

Figure 7 The Charge Generation of A PZT in
Ultrasound Wave.
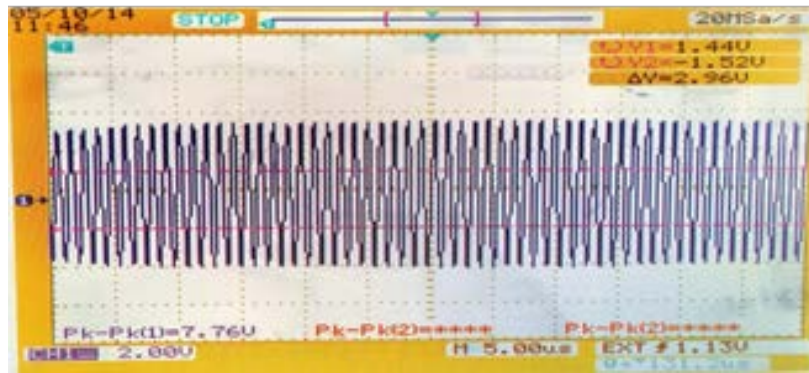
Figure 8 Waveform of the Voltage Output   of A Ultrasound Powered
Piezoelectric Element.

Design of the Micro Stimulator

The most common commercialized neural stimulator for pain management is the CNS stimulator that is implanted in the lower back for relieving chronic pain. However, modern electrical neural stimulators can also block pain by applying electrical current to PNS nerves. Typically a mille ampere or so of current passes through nerves but such that motor activation does not occur. The effective level of current is typically 75% of the motor threshold. At this point, the patient feels buzzing sensation that masks the sensation of pain coming from the portion of the extremity that is lower than the stimulation site. Commercialized neural stimulations generally run in 1 ms in a repetition rate ranged from 3-25 Hz with stimulation current up to 10 mA in some cases,

Commercial devices typically consist of two parts: the implanted pulse generator and electrode to the spinal canal. The pulse generators need to be recharged but generally under radio control of an external unit which can adjust the pulse parameters. These devices are usually implanted in the lower back and can be visually unpleasant and uncomfortable for the patient. Explantation of the electrodes and pulse generator can occur in the situation that the device is ineffective or patients do not tolerate it.

There is a significant advantage to small devices for PNS pain management because of a lower risk of their placement outside of the sensitive spinal canal and the neural cord that runs within it. Placement of bulky pulse generators in limbs, however, is often not practical because of their size and this has been a major disadvantage to the use of PNS.

This presented work seeks to investigate a neural stimulation design whose implantable portion is relatively small such that it does not require a silicone electrode wire and bulky pulse generator. The advantage of the system is the reduction of trauma of implantation and the externalization of the pulse generator and associated electronics so that they can be easily removed or upgraded.

The major challenges of making suitably small neural stimulator are to transfer sufficient energy through the skin in order to support the neural stimulation. Figure 9 shows the modality of the system. The electrical energy required for neural stimulation is relatively small, amounting to

15

several hundred microwatts. Such power transfer to an implanted device is relatively easily performed even with very small piezoelectric devices.

The proposed nerve stimulators are designed to be implanted in either side of the hind limbs near the sciatic nerve bifurcation, between the gastrocnemius and soleus. Upon the proper implantation of the stimulator, it will stimulate the sciatic nerve bundle nearby. The nerve stimulator can achieve different goals depending on its stimulation patterns. Larson and Towe (2011) achieved motor stimulation by using 100 micro seconds, 10 Hz stimulation pattern [8].
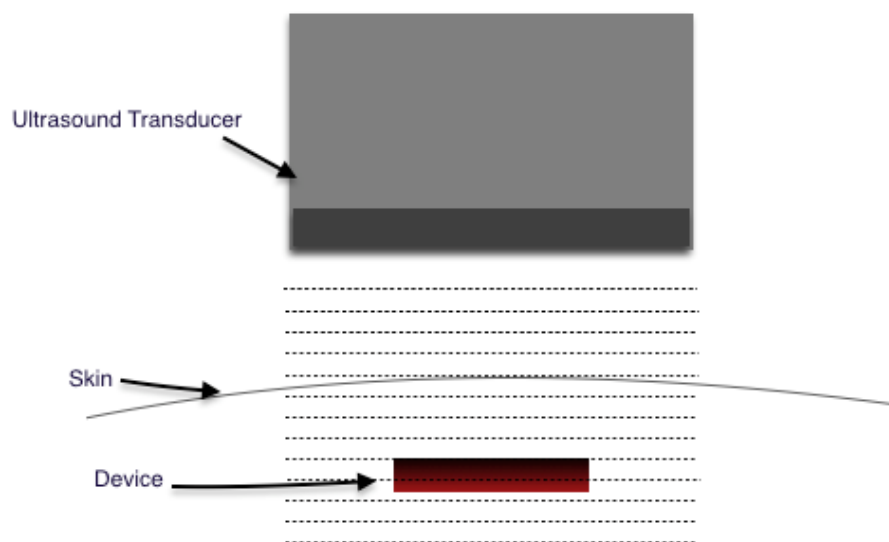
Figure 9 Stimulation System Modality.

An electrical stimulus can interact with the whole nerve bundle. In addition, large fibers are myelinated and faster in conducting impulses from the periphery to the brain, they are easier to be stimulated; the small fibers are unmyelinated, slower in conducting pulses, and more difficult to be stimulated. Therefore, it is possible to stimulate only the large fibers, such that the large fibers can activate the inhibition interneurons. That is, according to the gate theory, the afferent pain impulses will be blocked.

CHAPTER 3

METHODS

Components of the Stimulator

The neural stimulator devices are built based on a previous design [8], which is a circuit powered by piezoelectric components that transfer mechanical energy into electrical energy.
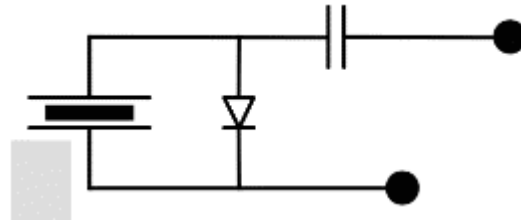
Figure 10 Schematic of the Neural Stimulator

The stimulator is consisted of three components (Figure 10). A PZT ceramic (PZT-5A), a Schottky diode(CDC 7630, Skyworks), and a capacitor. The PZT ceramic acts as a power supply to the nerve stimulator, and acts as a receiver to the external applied ultrasound.

The charge generation of the PZT is corresponding to the applied ultrasound, that is, when the PZT is in the ultrasound rarefaction zone, it will generate positive charges on the anode; when it is in the ultrasound compression zone, it will generate negative charges on the anode. As a result, the voltage ouput of the PZT actuated by the ultrasound will have the same oscillating pattern and frequency as the ultrasound, which is a biphasic AC signal. However, the sciatic nerve does not response to such high frequency biphasic AC current, the diode comes to place to rectify the current into a mono phasic current. The capacitor provides charge balance to protect the tissue.

An issue regarding the performance of this device is the diode threshold for rectification, that is, the applied voltage must be above about 150mV which is the characteristic of the employed Schottky diodes. Voltages below this are unrectified and therefore uneffective for neural stimulation.

17

The connections of the components are made by 10um gold wires and silver epoxy (H20E-HC EPO-TEK). Two 0.35mm platinum-iridium (85%-15%) alloy wires are used as bio-interface electrodes to reduce output port impedance and corrosion.

All the components of the device will be encapsulated into a polyamide tube (diameter: 1.04mm) filled with isolated hermetic medical grade epoxy (302-3M, EPO-TEK), leaving the bio-interface electrode exposed. Since the components are in ultra small sizes, the fabrication are processing under a 10x microscope.

Figure 11 shows the employed nerve stimulator.
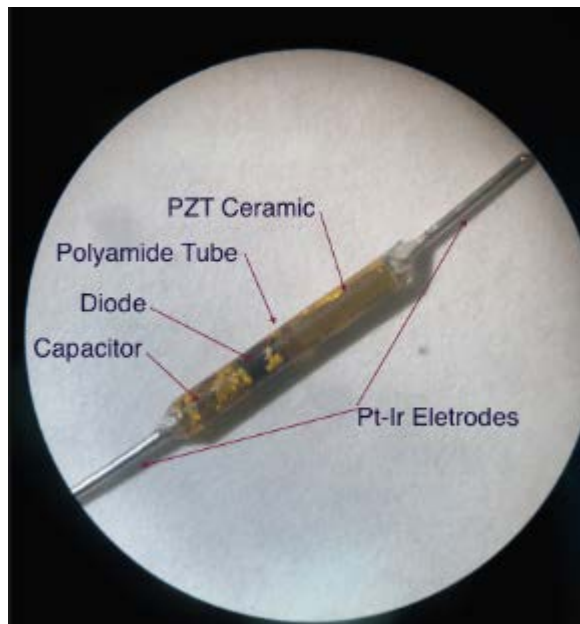
Figure 11 A Completed Device.

The Problem of Angular Sensitivity

A significant problem arises in the practical utilization of implantable biomedical devices powered by ultrasound energy. In that, acoustic wave interfacing can compromise the energy transfer process. When a piezoelectric ceramic is placed in pressure wave, the polarity of charge generation depends on whether the piezoelectric ceramic is in the rarefaction zone or the compression zone. When the PZT is in a compression zone, the positive face of the PZT generates positive charge while in a rarefaction zone it generates negative charge. This becomes a problem when part of the PZT is in the rarefaction zone and part of it is in the compression zone, the opposite charges generated from different parts of the PZT will cancel out each other. So the total charge output will be dramatically decreased.

Thus, the voltage of the PZT will be highly depends on the ultrasound receiving angle, the PZT size, and the ultrasound frequency. The wavelength of the sound can be calculated by

$$\lambda = \frac{v}{f}$$

where λ is the wave length, v is the speed of the sound in the corresponding, f is the frequency.

Table 2 is the speed of sound in different medium.

Medium	Speed of Sound(m/s)	Temperature (Degree Centigrade)
Air	343	20
Water	1498	25
Blood	1570	37
Muscle	1580	37
PZT	3970	20

Table 2 Speed of Sound in Different Medium

As we are only considering the ultrasound in PZT, the half wavelength of the sound is about 2mm when the ultrasound is in 1MHz. Thus, the higher the frequency, which has the shorter wavelength, the greater possibility of cancellation on a device than one with a relatively larger length compared to the half wavelength.

There are several approaches to alleviate such a situation: decrease the frequency of the ultrasound, that is, to increase the wavelength of the pressure wave, which will increase the

19

possibility that the whole peace of the PZT is in the same pressure zone. Decreasing the size of the PZT ceramic, will also increase the possibility that the whole piece of the PZT is in the same pressure zone. In addition, align the ultrasound traducer will help to make sure the sound wave propagation direction is parallel to the PZT poling direction.

Since the thickness of the PZT used is about 0.48mm and much smaller than the half wavelength, we can ignore the transverse cancellation effect and only consider the longitudinal cancellation, since the length of the PZT ceramic will exceed the half wavelength in most of the cases.

Matlab Model for Angular Sensitivity

To computationally model the angular sensitivity of the PZT, a Matlab program was developed to demonstrate how the receiving angle, ultrasound frequency, and PZT size affects the output. This program calculates and plots the normalized output of the PZT with different ultrasound incident angles. The script of the Matlab program is attached in appendix. Figure 12 shows the diagrammatic Drawing of the PZT and ultrasound.
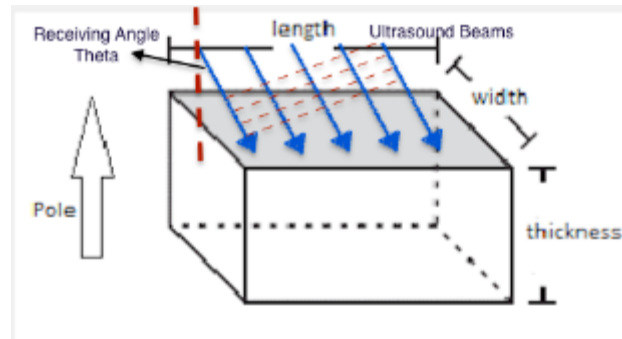
Figure 12 Diagrammatic Drawing of the PZT and Ultrasound

This section investigates the output of the PZT when there's a rotation around the long axis. The rotation modality is shown in Figure 13. In this type of rotation, the PZT may work in two types of operation mode, g_{33} mode and g_{31} mode, that is, the longitudinal mode and transverse mode. It is mentionable that g_{33} and g_{31} constants have opposite plus-minus signs, which means when the ultrasound receiving angle is not a right angle, the PZT will operate in both g_{33} mode and g_{31} mode, because of the opposite signs, a considerable portion of the charge generated by these two operation modes will cancel each other.
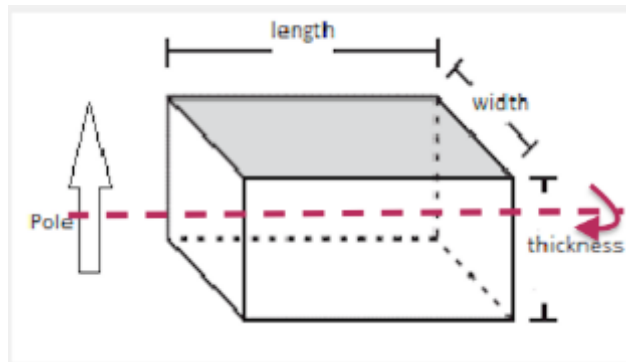
Figure 13 Rotation Around the Long Axis

Since the width and the thickness of the PZT ceramic are both smaller than the considered ultrasound half wavelength, there will not be cancellation in those directions inside the PZT in rotation around the long axis. The only cancellation we need to consider is the cancellation between g_{33} operation mode and g_{31} operation mode. When the ultrasound is hitting the coated side where the receiving angle is parallel to the poling direction, the PZT works in g_{33} mode; when the ultrasound is hitting the uncoated sides to where the receiving angle is perpendicular to the poling direction, the PZT works in g_{31} mode. Assuming there is only rotation around the long axis occurring, the normalized open circuit voltage generated by g_{33} mode can be obtained by V_{ 33 }=F*cos(\theta)*{ g }_{ 33 }.

$$V_{33}=F*cos(0)*g_{33}$$

The voltage generated by g₃₁ mode can be obtained by $V_{33} = F*\sin(\theta)*{g}_{31}*\frac{Thickness(charging\quad direction)}{Width(Neutral\quad direction)}$.

$$V_{33}=F*sin(\theta)*g_{31}*\frac{Thickness(charging\ \ direction)}{Width(Neutral\ \ direction)}$$

The total output can be obtained by adding up them together.

$$V=F*sin(\theta)*g_{31}*\frac{Thickness(charging\ \ direction)}{Width(Neutral\ \ direction)}+F*cos(\theta)*g_{33}$$

Rotation around Short Axis

This section investigates the output of the PZT when there's a rotation around the short axis. The rotation is shown in Figure 14. In this type of rotation, the PZT will also work in two types of operation modes, g_{33} mode and g_{31} mode, while rotating around the short axis. However, in this situation, the thickness of charging direction is much smaller than the thickness of neutral direction (about 10 times smaller). In addition, the g_{31} factor is about half of the g_{33} factor on value, so the effect of the g_{31} operation mode is negligible when considering the rotation around short axis.
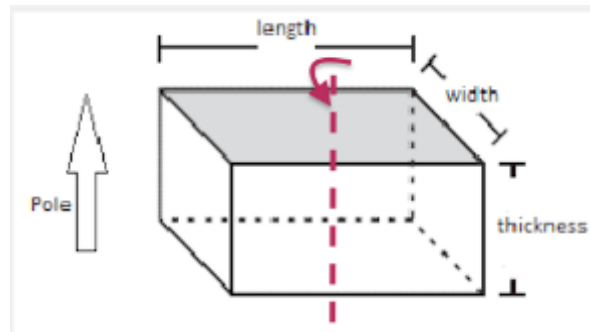
Figure 14 Rotation Around Short Axis

However, since the lengths of the devices are varied from 2-4mm, which are larger than the half wavelength of the employed ultrasound. The charges generated in rarefaction zones will cancel the charges generated in the compression zones. The working length of the PZT is calculated by $Length_{working} = Length * cos\theta$.

$$Length_{working} = Length * cos\theta$$

The possible cancellation zone in wave propagation direction is calculated by $Length_{possiblecancellation} = Length * sin\theta$

$$Length_{possible-cancellation} = Length * sin\theta$$

By calculating the remainder of the half wavelength dividing the working length, we can obtain the non-cancellation length of the system. Since the divider is half wavelength, the non-cancellation length can not exceed the half wavelength of the employed ultrasound. Therefore, the output normalized by the maximum value, which is when the ultrasound incident angle is 90

degree, is calculated by

{ V }_{ output }=\frac{ { Length }_{ none-cancellation } }{ { Length }_{ possible-cancellation } }

*{ Length }_{ working }/Length.

$$V_{output} = \frac{Length_{none-cancellation}}{Length_{possible-cancellation}} * Length_{working}/Length$$

Effect of Piezoelectric Device Size

        To test the maximum outputs of the PZT ceramics in different sizes, five pieces of PZT
ceramics in different sizes are encapsulated in polyamide tubes using hermetic epoxy. In addition,
the copper wire electrodes on each device are exposed in order to be connected to the
oscilloscope. Figure 15 shows the completed devices.
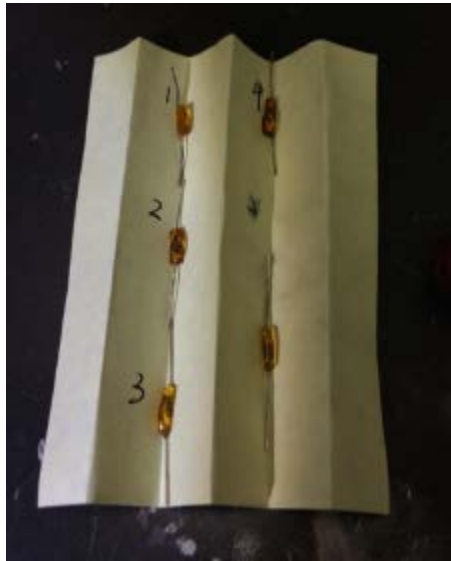
Figure 15 PZT Ceramic in Different
Sizes
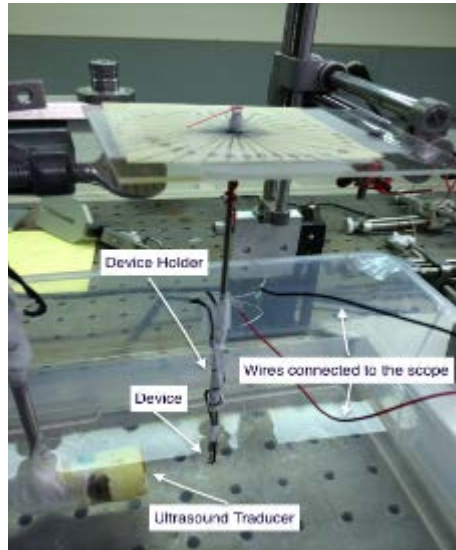
Figure 16 PZT Ouput Test Set Up

        These testing devices are respectively soaked into 1.7mS/cm water and excited by
945kHz ultrasound using the same set-up. The testing set up is show in Figure 16. The ultrasound
traducer is connected to a pulse generator, which is generating 100V single pulses, with 100uJ
energy. Figure 17 is the output pattern shown on the oscilloscope of one of the devices.
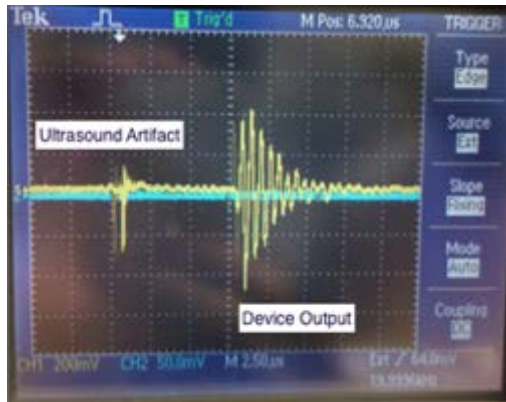
Figure 17 PZT Output Waveform

Table 3 shows the output of the devices and their sizes.

Devices Number	Width(mm)	Length(mm)	Thickness(mm)	P-P Output(mV)
1	0.42	2.98	0.48	340
2	0.59	2.90	0.48	350
3	0.74	3.07	0.48	500
4	0.86	3.11	0.48	620
5	0.97	2.97	0.48	800

Table 3 Different Output Corresponding to Different Sizes of PZT

Based on the output of the test devices and the stimulator size requirements, the size of 0.74*3.07*0.48 is selected.

Fabrication Procedure

Step 1:

a. Use the 602M Dicing Saw to cut the commercial Piezo System, 0.5mm thick, 3 inches

by 3 inches piezoelectric ceramic plate.

Figure 18 Diamond Dicing Saw

b. Use grinder to grind the diced PZT ceramic pieces into desired sizes.
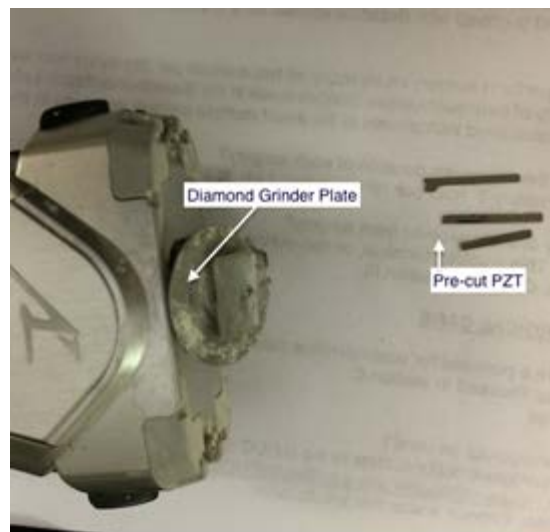
Figure 19 Diamond Grinder For Accurate Sizing

c. Use grinder to grind the diode package until it can easily fit through the polyamide tube.
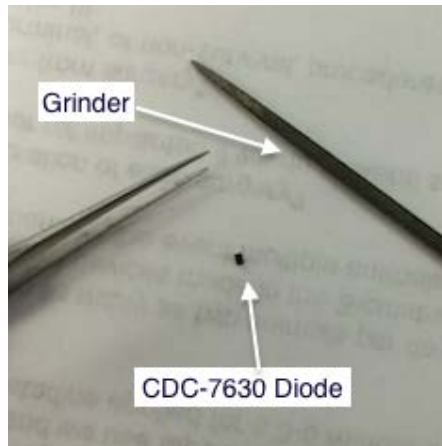
Figure 20 CDC-7630 Diode

Step 2:

a. Under 10X microscope, connect the components following the schematic using silver epoxy and gold wire.
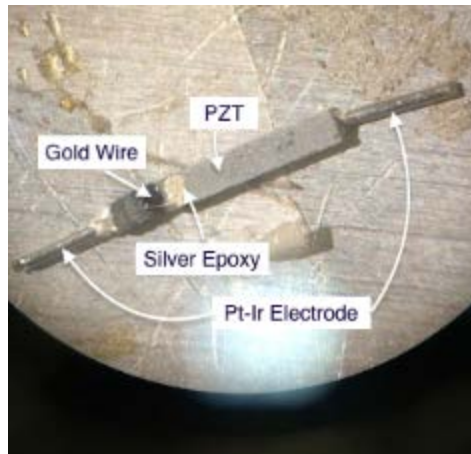
Figure 21 Device Before Encapsulating

b. Put the soldered components into 175 degree centigrade oven to cure for 30 min, in order to harden the silver epoxy. To eliminate short circuits and to improve the compaction of the devices, the hardening of the epoxy should be performed respectively for each connection.

Step 3:

Carefully place the connected components into the polyamide tube, properly mix the hermetic epoxy and inject the epoxy into the tube carefully, make sure there are no bubbles in the

tube. Place the device on a holder and put it into 65 degree centigrade oven for 3 hours in order to

harden the hermetic epoxy.
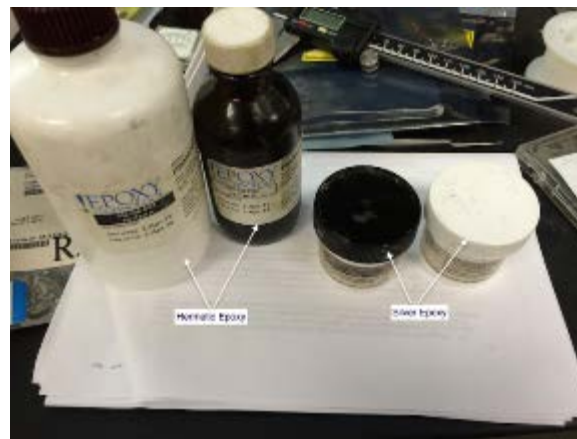
Figure 22 Silver Epoxy and Isolated Epoxy

Figure 23 Device Fit Through Polyamide
Tube

Animal Model

The characterization and quantification of pain threshold in animal models has been addressed by a number of investigators, and has been reviewed by Bolcskei et al [20]. Traditional approaches to qualify pain threshold include but not limited to constant temperature hot plates, tail clips and plantar tests. However, those approaches can be largely affected by the latency of the withdraw movement and the irrelevant movements of the rats'. The task is to find a repeatable but humane way to assess the pain relief effect by the neural stimulation. Of all the method outlined by Bolcskei et al, this research selects a ramping temperature water bath, as it is the most appropriate and achievable approach in this laboratory. This approach was reported to produce a reproducible indication of the discomfort threshold, and has been adopted by a number of investigators in this field and so is an acceptable model. The model employs a physiological withdraw reflex response to a threshold temperature, such reflex is highly reproducible and safe for rats. The expectation is that the threshold temperature of such rat withdraw reflex from the warming water would vary by the effectiveness of the neural stimulation in suppressing pain. Thus, this model is employed in this work as an indicator for the function of neural stimulator in relieving pain. Since the leg pain caused by PVD is a burning sensation, such burning sensation is similar to the situation when the leg is soaked in heated water, we expect this approach can well qualify the function of the nerve stimulator.

When we conduct the experiment, either of the rat's hind limb is soaked into the warming water tank. The uncertainty of the withdraw movement can be triggered by other factors include but not limited to the handle gestures, the noise of the environment and the condition of the rat at that time. To reduce uncertainty, the heated speed of the water should be properly set, that is, the experiment duration should be in a range in which the withdraw movement only responses to the thermal stimulus.

This approach has been reported to have an improved sensitivity and reproducibility in the measurement of discomfort threshold. Such improvement was attributed to the limitation of the noise; and the activation of c-fibers without actuating the nociception receiver.

31

CHAPTER 4

RESULTS

Computer Model Result

The graphical interface of the computer model of the performance of the PZT stimulator is shown in figure 19. It illustrates that the intensity of the output of a PZT is a function of the size of the PZT and the incident angle. The investigation uses different parameters to evaluate the output of the PZT such as length, thickness, width and ultrasound frequency.
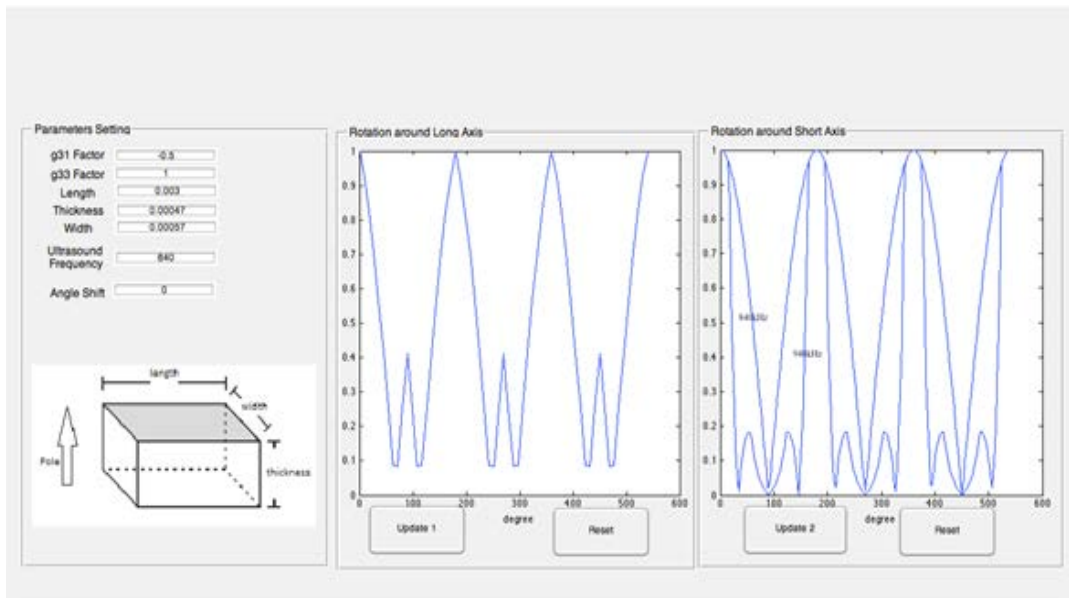
Figure 24 User Interface of the Computer Model

The models show that for a fixed thickness of the PZT, in one trial, the length of the PZT is fixed at 3mm because this is the most used length in our application. The PZT widths and ultrasound frequency are variables. According to the calculation of the non-cancellation length equations for rotation around short axis, width is not involved in the equation, only the change of ultrasound frequency may affect the result.

The width of the PZT ceramic will not exceed 0.8mm due to the constraint of the polyamide tube, furthermore, we will not use an ultrasound transducer with a frequency higher than 2MHz due to the constraint of laboratory instruments. Even in the scenarios that we use the 2MHz transducer, the half wavelength is 1mm, which is larger than both the width and thickness of

our devices. That is, there will not be any serious cancellation in the PZT due to the high frequency.

In Figure 25, the widths of the device is 1mm, 0.6mm and 0.4mm.
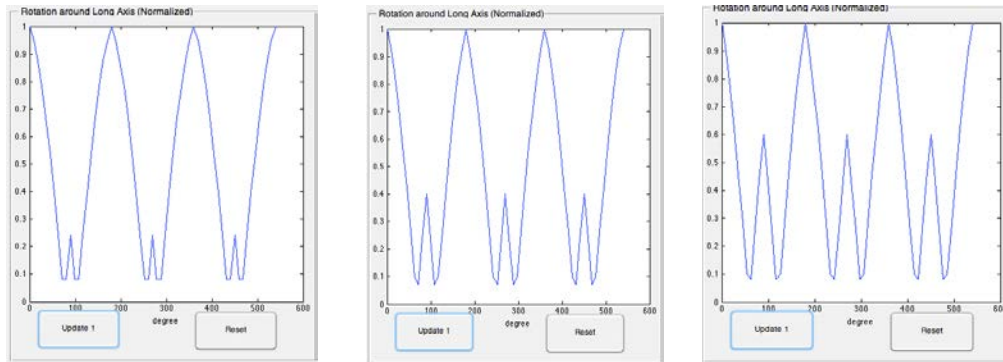
Figure 25 Output Depends on Rotation Angle Around Long Axis When Width is 1mm, 0.6mm and 0.4mm.

In assessing the angular sensitivity around the long axis, we only consider the effect of the change of the width; the length and the thickness are held constant. As we can see from the figures, the smaller the width, the higher possibility the device can give a more than 50% output. The higher peaks in the figures represent the situations when the ultrasound beams are hitting directly on the charging surfaces, the lower peaks represent the situations when the ultrasound beams are hitting directly on the unelectroded side. The dips showed the total cancellation when the ultrasound beam is hitting obliquely from 0 degrees to 90 degrees.

The angular sensitivity will decline following the decrease of the width, because the smaller the width is, the higher output we can get from the g31 operation mode, according to the following equation.

$$V_{33} = F * sin(\theta) * g_{31} * \frac{Thickness(charging \ direction)}{Width(Neutral \ direction)}$$

When considering the rotation the short axis, the frequency of the ultrasound is the only variable. Figure 26 and Figure 27 show that the highest output occurs when the frequency is low enough to have a larger half wavelength than the length of the PZT. The number of the peaks and dips increase following the increase of the ultrasound frequency because there are more possibility for total cancellation. In addition, following by the increase of the frequency, the working

33

length of the devices will decrease since it is correlated to the half wavelength, as shown in the following equation,

$$Length_{working}=Length*cos\theta$$

As the theta increases, the working length decreases resulting in a reduction of power.

Figure 26 and figure 27 showed the output characteristics of the devices when actuated by different frequencies of ultrasound.
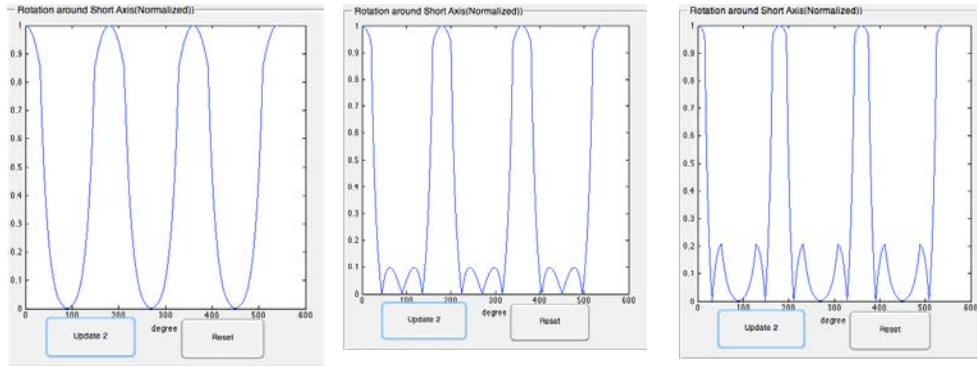
Figure 26 Output Depends on Rotation Angle Around Long Axis When the Applying Ultrasound Frequency is 500 kHz, 750 kHz and ! Mhz
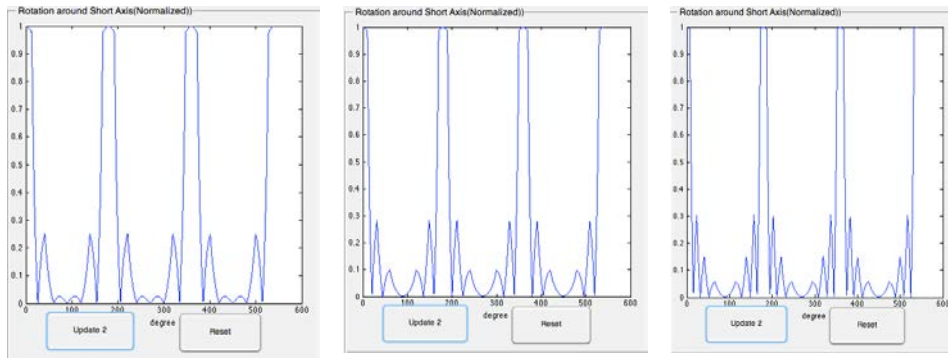
Figure 27 Output Depends on Rotation Angle Around Long Axis When the Applying Ultrasound Frequency is 1.2MkHz, 1.5 MHz and 2 Mhz

To evaluate the function of the constructed neural stimulator, a series of in vitro experiments were conducted to assess the voltage output, current generation, and the angular sensitivity of the constructed prototype devices.
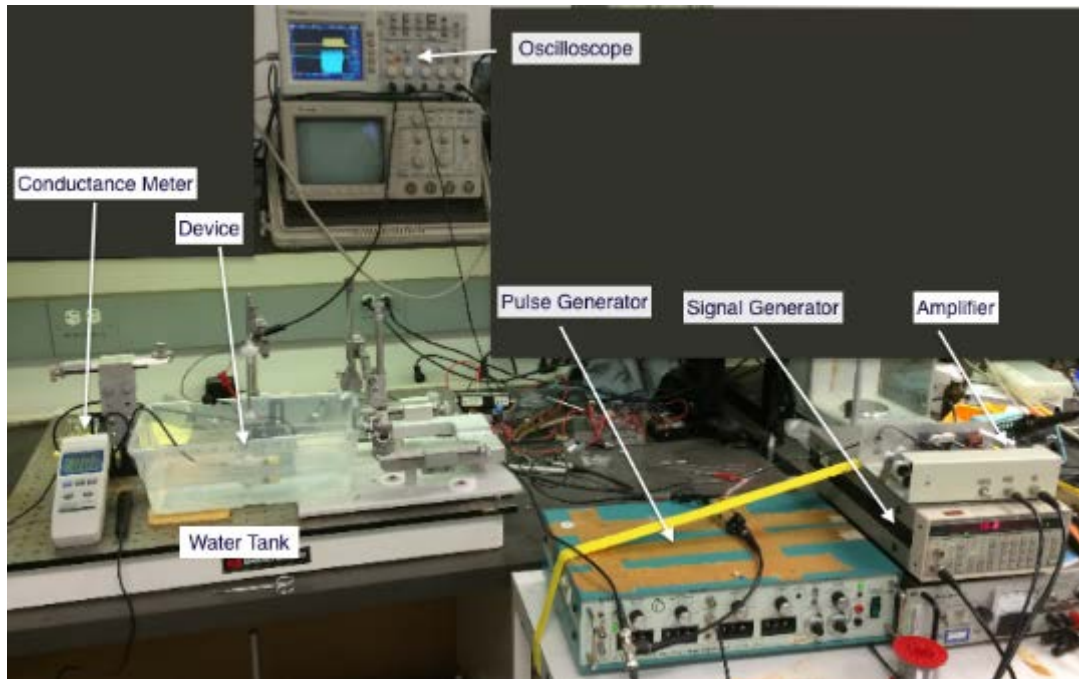
Figure 28 Experimental Setup for In-Vitro Experiment

Multiple ultrasound transducers with different frequency were employed in in-vitro experiments. A signal generator gated by a pulse generator activates the ultrasound driver, which is a class C amplifier. The signal generator was set to the ultrasound transducer resonance frequency, the pulse duration and repetition rate were set on the pulse generator, the ultrasound intensity was adjusted by setting the voltage applied to the transducer. CH1 of the scope was connected to the submerged stimulator by wires to detect the voltage output of the device, CH2 of the scope was connected to the output of the class C amplifier with 20 dB attenuation to monitor the voltage across the ultrasound traducer. The experimental set up is shown in Figure 28.

The neural stimulator used in the in-vitro experiments was shown in Figure 29, the 10mm long device can fitted through a 18 gauges syringe needle. The neural stimulator and the ultrasound transducer were completely immersed in a water tank, the device was attached to a

holder, as Figure 30 shows, it has two leads connecting the device's electrodes to the scope. Two cuffs were used to ensure the fine connections between the wires and the stimulator electrodes. Furthermore, a conductivity meter was employed to measure the conductance of the water.
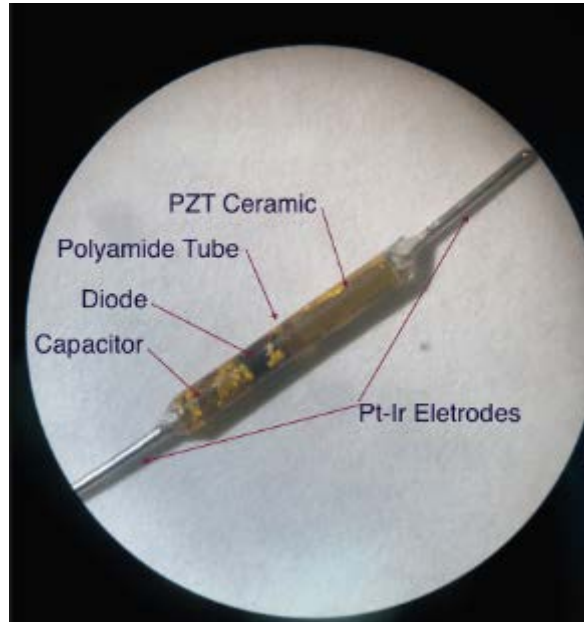
Figure 29 Employed Device
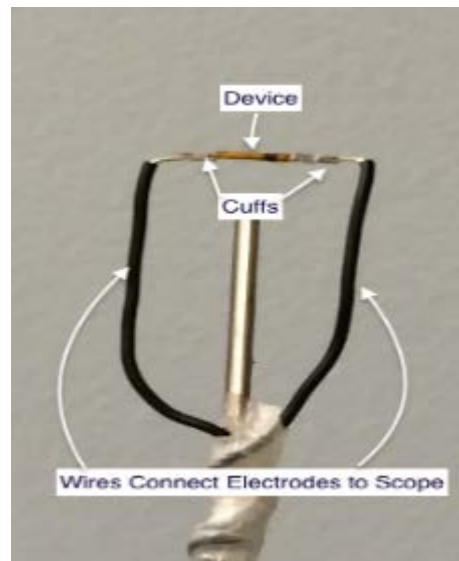
Figure 30 Device Holder
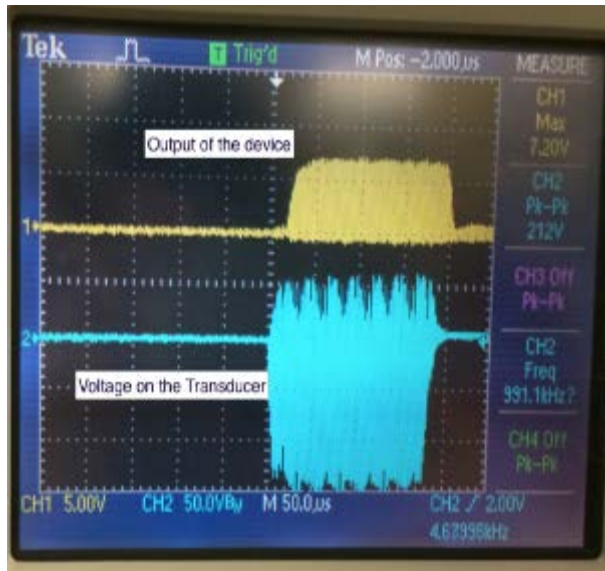
Figure 31 Device Output Waveform

Figure 31 shows the output acquired from the oscilloscope. We can see that the output of the PZT has been successfully modulated into a mono phasic output that would be sensible by the nerve tissue. And the diode threshold is estimated to be about 150mV from the oscilloscope.

<center>Output Dependence on Conductivity</center>

The voltage output of the device and the current through the devices depends on the conductance of water. It is also varied to mimic biological internal environment, which in turn depends on the implantation sites.

The pulse generator which amplitude modulates the signal generator generated a 200ms pulse with a repetition rate of 10 Hz while the amplifier amplifies the modulated tone burst signals to peak to peak 212V, which then drives the ultrasound transducer at its nature frequency, 940kH. The conductance of water was monitored as a variable and modified by adding salt in it. The experimental set up is shown in Figure 32.
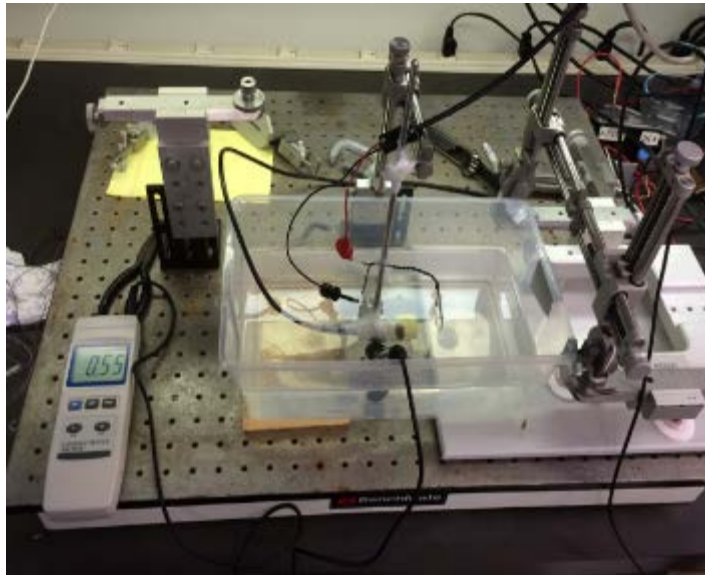
Figure 32 Experiment Set Up for Measuring Output Dependence for Conductivity.

As seen in Figure 33, the output of the PZT has dropped when the conductivity changed from 0 to 4 mS/cm, and reached a plateau when the conductance was 6 mS/cm and above. Since the device will be implanted in the muscle, the conductance of the muscle at the given frequency (940Hz) is about 4.9mS/cm, where the electrode impedance is estimated to be about 2k ohm. In such condition, the output of the device is about 1.5V; as a result, the stimulation current can reach 750uA which is enough to stimulate the nerve for this given stimulation duration.
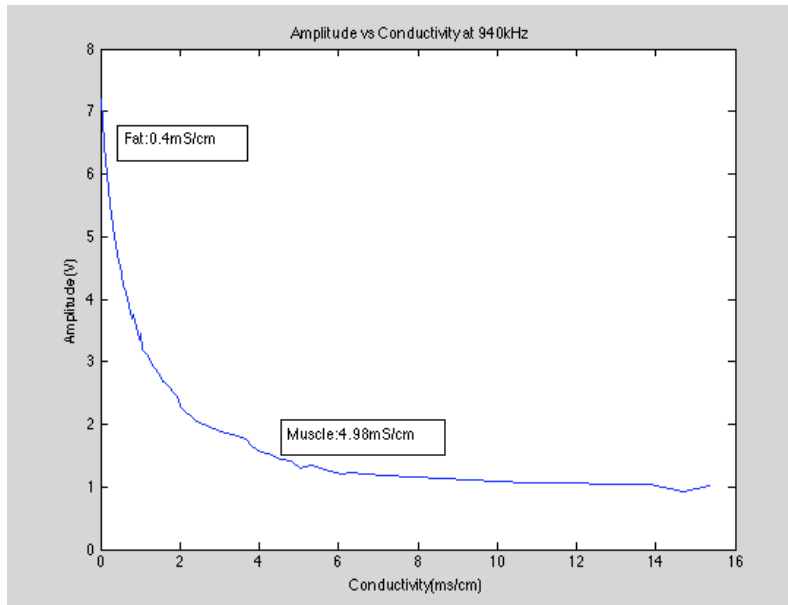
Figure 33 Device Output Depends on Conductivity of the Environment.

Output Dependence on Driving Voltage on Ultrasound Transducer

To evaluate the device output as a function of driving ultrasound power, the voltage drive was increased by a series of steps and the resulting stimulator output voltage. The experiment set up can be seen in Figure 34 whereas Figure 35 depicts the ultrasound output dependence on the driving voltage.
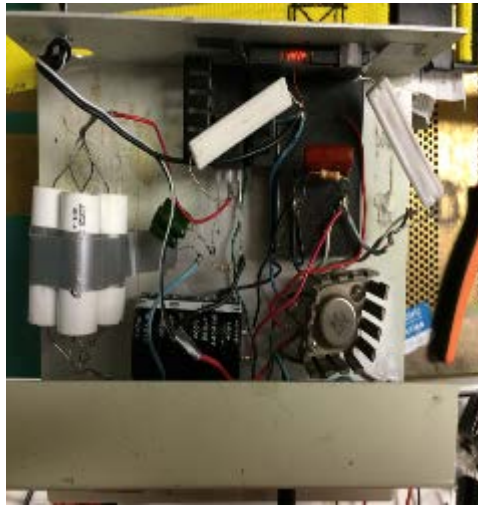
Figure 34 Ultrasound Driver and Power Supply
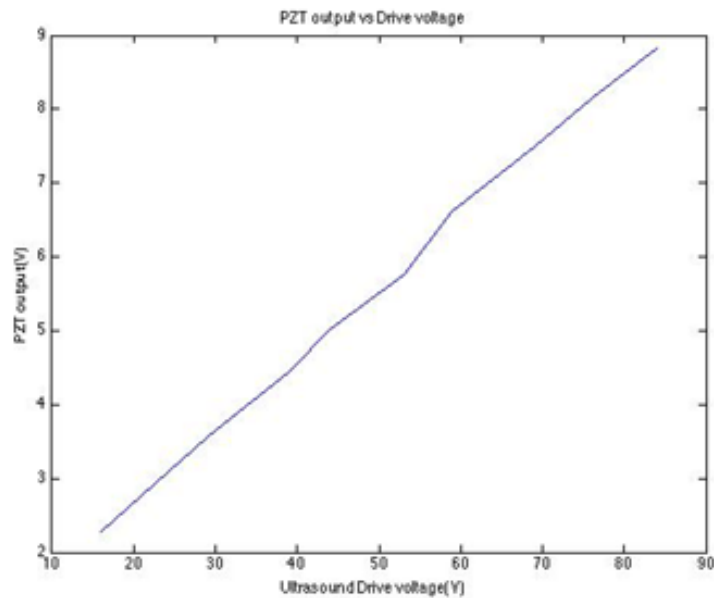
Figure 35 Device Voltage Output Depends on Ultrasound Driving Voltage

Angular Sensitivity Experiment

To assess the angular sensitivity of the devices as discussed in chapter 3, the neural stimulator is varied with respect to the ultrasound transducer direction. The experiment set up is shown in Figure 36 and the resulting output is shown in Figure 37 and Figure 38.
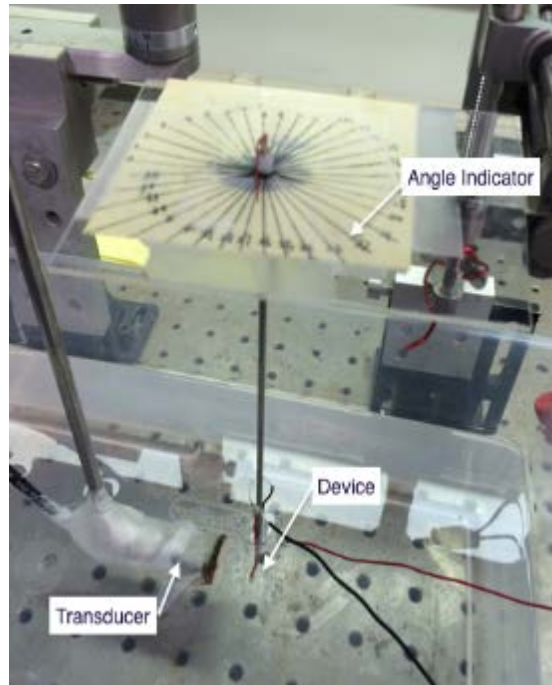
Figure 36 Angular sensitivity set up

Figure 37 shows the voltage output of the device when it rotated around its long axis. The experiment data were consistent with the Matlab model. The peaks of the output were corresponding to the situations when the ultrasound was hitting directly on its electroded or unelectroded sides. Since the g_{31} and g_{33} value have the opposite positive-negative sign, the four dips were corresponding to the situations when the ultrasound was hitting on both the unelectroded and the electroded sides with an ultrasound incident angle where the charges had the maximum cancellation.
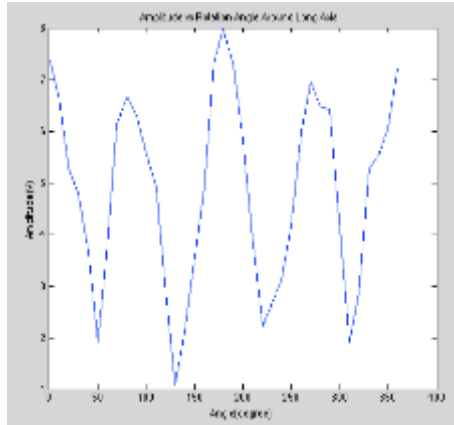
Figure 37 Device Output Depends on
Rotation Angle Around Long Axis

Figure 38 shows the angular sensitivity of the device when it rotated around its short axis.

The experiment data were also consistent with the Matlab model. The two higher peaks

represented the situations when the ultrasound propagation direction was parallel with the poling

direction of the PZT. The dips represent the situation when the charges were cancelled out.
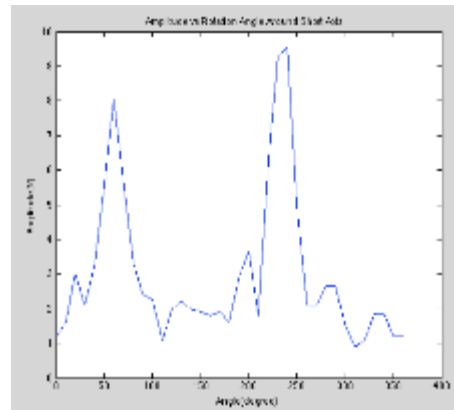
Figure 38 Device Output Depends on
Rotation Angle Around Short Axis

Remote Detection of the Implant Functioning

It is desirable to be able to detect the functionality of the neural stimulator remotely from the implant site such from the surface electrodes which detect the skin potential generating from the implant. This allows the assessment of the location and the change of the performance of the devices over time from an electrical point of view. Furthermore, this will provide insight into whether it loses its function in electrical or physiological process. Making the device small can reduce trauma as well as angular sensitivity performance; however, this will reduce the volume conductive signal remotely detectable by the electrodes on the skin. It is of interest then to understand how the remotely detected signal changes as a function of the electrode separation distance and the distance between the surface electrodes and the device.

An experiment was thereby to evaluate how the distance between each of the surface electrodes and the depth of the device affect the voltage acquired at the surface electrodes. The amplifier drove a modulated tone burst signal at peak to peak 212V at 940kHz which is the transducer's resonance frequency. Figure 39 illustrates the experiment set up for the surface electrodes evaluation.
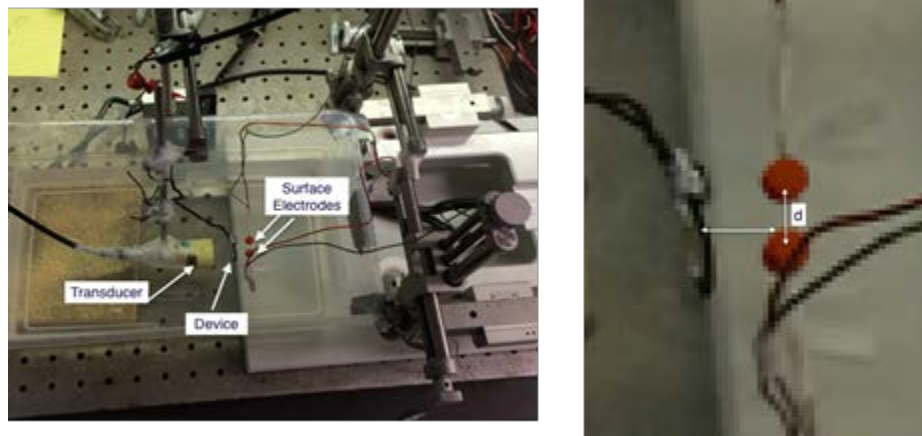
Figure 39 Remote Detection Experiment Set Up
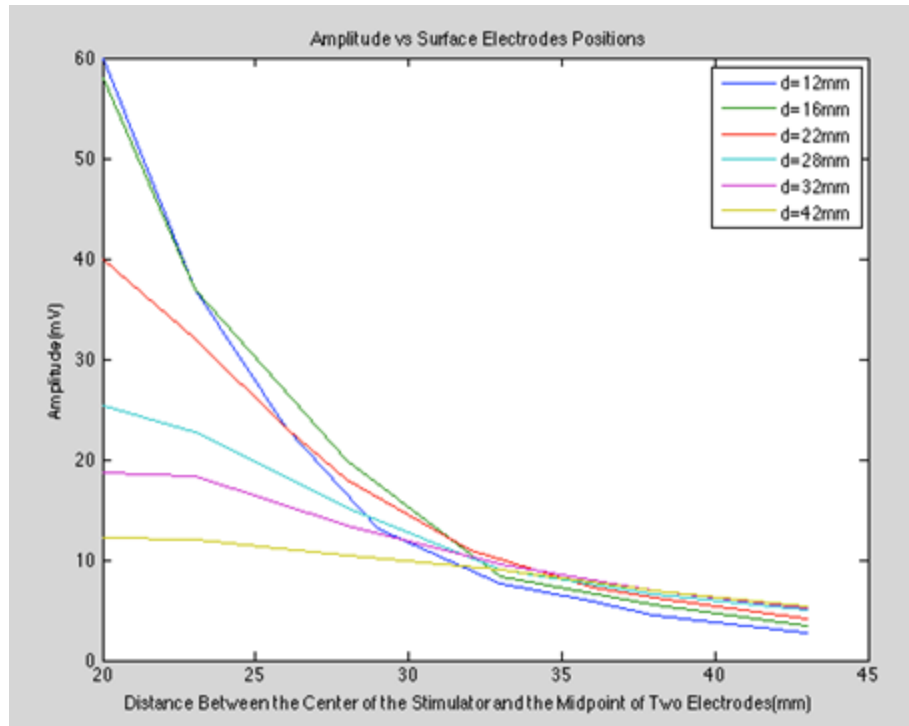
Figure 40 Remote Detected Voltage of the Device

As we can see from Figure 40, for a given L (depth), the detected output of the remote electrodes decrease as the distance between the two electrodes increases. For a given d (electrode distance), the output decrease as the distance between the device and the electrodes increases.

Feasibility of Ultra-small Neural Stimulator

The models and tank data clearly showed that the desirability of making ultrasound powered neural stimulator as small size as possible, consistent with sufficient current capacity to stimulate the nerve. It is known that neural stimulation occurs at much lower current when electrodes are placed intra fasicularly. This suggests that the piezoelectric neural stimulator of this design of micro scale stimulator may still have the ability to generate the current so as to be useful in block pain in PVD. The shortcoming is that more invasive surgery will be required.

To assess the potential of this very small nerve stimulator, an evaluation of the very small piezoelectric element was conducted to assess their output at higher ultrasound frequency. The prototype devices are shown in Figure 41.
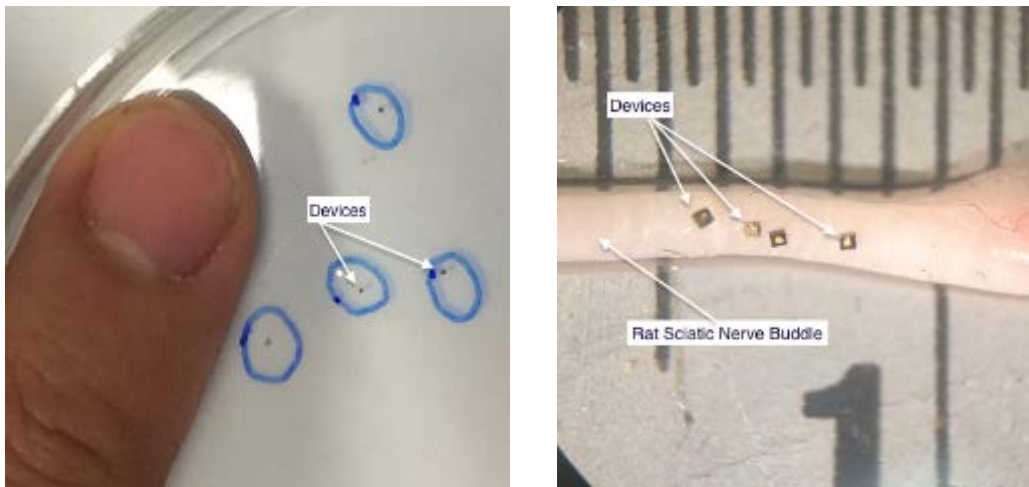
Figure 41 Ultra Micro Scale Device Compared to Finger and Rat Sciatic Nerve

A CDC-7630 diode (300um*300um) die was stacked on a PZT chip (300um*300um) cut by commercial saw. The connection between the PZT and the diode die was made by silver epoxy.

A 5Mhz transducer driven by a 100V single pulse using the Panametrics Inc. computer-controlled Pulser/Receiver was used to stimulate the micro PZT chip. While the PZT chip was placed on the focal spot of the traducer, the PZT chip in different loads gave outputs as shown in Figure 42.

This result shows that 300*300 um piezoelectric material can provide output voltage that will overcome the diode threshold voltage and thus provided relatively low level of stimulation current. The output port impedance as shown in the plot is considered low and consistent with that of bio-interface electrodes.
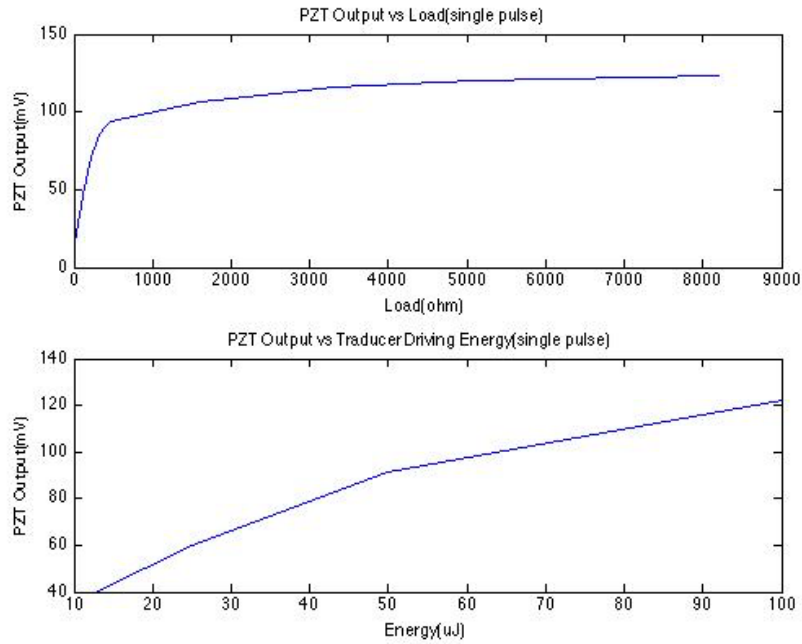
Figure 42 Ultra Small Device Output

Test in Rat

The device was first tested in a rat carcass, using the same set up and parameters used during implantation in living rat. As shown in Figure 43, the device was placed in the implantation site while still connected with wires to the oscilloscope. The incision of the dead rat is filled with saline to best mimic the real situation.
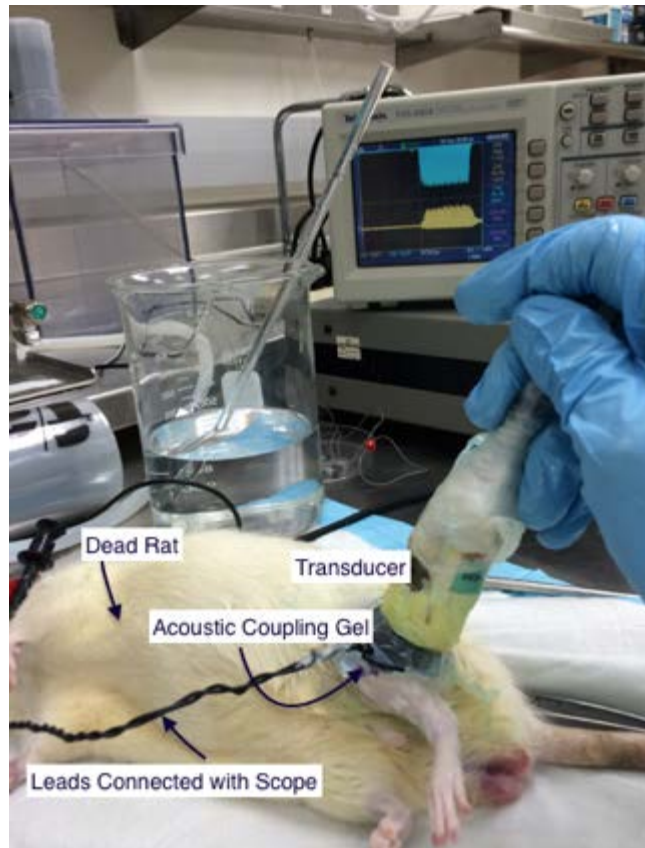
Figure 43 Rat Body Experiment Set Up

This result showed a high sensitivity to the transducer position with the implant output voltage varying from 1V to 4V while the typical values were between 2V and 3V. However, the angular sensitivity was not as serious as expected due to the small size of the device. This output was favorable for expecting an implanted device to stimulate the nerve.

In Vivo Experiments: Hot Water Bath Experiment

To assess the ability of the prototype neural stimulator to relieve pain and the clinical situation, the in-vivo experiments were conducted using Sprague-Dawley rats. The experimental protocol requires that the researcher must accommodate the rat to be able to be handled for a 2-3 minutes test period where their hind limbs were introduced to warm water. This protocol, which consists of daily handling interaction with the rat prior to the neural stimulation study as seen in Figure 44, was approved by the ASU IACUC..

Figure 44 Rat Handling Interaction

Figure 45 presents a constructed experimental setup consists of a magnetically stir water bath whose temperature was controlled by three immersion heaters connected to a Variac. The experiment initially used a PID controller attempt to control the temperature in real time; however, it was too slow and later was abandoned. The temperature was then manually controlled. We used a water tank to soak the rat's hind limb and a stirrer to stir the water to achieve equally heated of the water as Figure 34 shows. The protocol required water to be heated up at a speed of 0.33 degree/ second centigrade from 30 to 50 degree centigrade. As a result, it took about 60s for the system to heat the water from 30 to 50 degree centigrade.
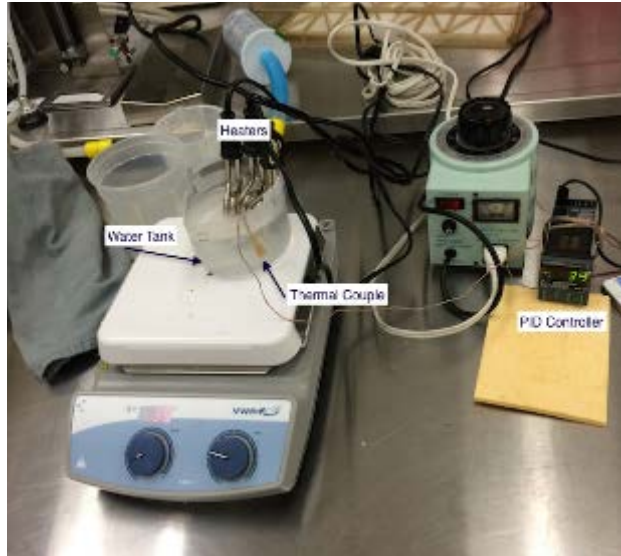
Figure 45 Hot Water Bath Experiment Set Up

Before the implantation of the devices, a series of hot water bath experiments were conducted to obtain the baseline withdraw threshold indicated by temperature. The entire procedure depended on the rat being corporative and not violently squirming over at least for 60 seconds during the test. In order to make the rat at ease to be held by hands, the rat was handled everyday for 5 minutes each time, 5 times in total, and by the end of each handling task, the rat was fed with treats. The training of the rat continued for 3 weeks. By the end of the training, a series of tests were done by holding the rat and soak one of its hind limb into 36 degrees centigrade water. The finding was that after the 3-week training period, the rat could be held steadily without any sudden movements typically for more than 50s in series

Since the proposed implantation site will be the left hind limb of the rat, the hot water bath experiments were conducted only on the rat's left hind limb. The rat's hind limb was soaked into the water when its temperature was heated to 33 degree centigrade. The duration of the experiment and the temperatures when the rat's withdraw reflexes occurred were recorded while there was a 5 minute interval between each trial. The data are shown in Table 4.

Trial Number	Starting Temperature (Degree Centigrade)	Experiment Lasting Time (Second)	Withdraw Temperature (Degree Centigrade)
1	36	25	44

2	32	35	44
3	36	25	44
4	37	24	41
5	33	38	45
6	34	38	44
7	32	45	46
8	33	45	46
9	34	45	46
10	35	44	45
11	36	40	44

Table 4 Rat discomfort threshold baseline before surgery

The result shows a relatively stable withdraw temperature between 44 and 46 degree centigrade. We assumed that the temperature threshold of the rat's left hind limb is 45 degree centigrade. Another series of experiments were performed after the implantation of the devices.

Surgically Implanting the Stimulator

The neural stimulator was surgically implanted into the left hind limb of a 630g Sprague-Dawley rat along the sciatic nerve following an IACUC approved protocol. The rat was anesthetized by administering the anesthesia respirator using 3% isofluorane, to reduce the discomfort and the risk of inflammation of the rat during the surgery. Subcutaneous injections of Bupenorphine, Molaxacan and Clavamox were administered pre-surgery. Upon reaching a stable condition on the operating platform, the area to be operated was shaved to expose the skin. The area of the skin that was to be opened as well as a radius of 2-3 cm outside of the planned location of incision was sanitized and cleaned by using iodine swab and alcohol. Pinch test on the rat's paws were applied to verify the anesthetization of the rat.

As shown in Figure 46, a 1.5cm incision was made on the lower to mid-thigh on the left side of the rat using a scalpel. The muscle under the subcutaneous tissue was exposed using a hemostat. A gap between the posterior compartments was exposed, and separated gently to expose the sciatic nerve bundle. The device was then placed along the nerve bundle using a tweezers.

Figure 46 The Surgical Incision

The muscle and the skin were then sutured up using dissolvable suture. Anesthesia respirator was removed after the surgery, and the rat was returned to it living quarter.

Bupenorphine was administered to alleviate discomfort every 12 hours for 3 times, Molaxacan and Clavamox was administered as an anti-inflamatory every 24 hours for 5 days.

After we confirmed that the rat was fully recovered, ultrasound therapy was administered and we observed consistence muscle twitching from a relatively wide range of incident angles. The implantation of the neural stimulator was determined to be successful.

Rat Neural Stimulator Results

A difficulty with the assessing the neural stimulator performance in pain relief is the problem of introducing the stimulation therapy for a period of 10 min in an awake rat. This required that the ultrasound transducer must be held in contact with the inguinal region of the rat leg during the energy transfer to the implant. However, the literature shows that neural stimulation can have persistent affects for at least 30 min and as much as an hour after the remove the therapy [20].

The only way of conducting the experiment proved to be the use of anesthesia to immobilize the rat while ultrasound was applied. This is undesirable because there is possibility that the anesthesia itself could be affecting the discomfort threshold for some unknown time upon the recovering of the rat while it is awake. So the protocol consists of trials of several sessions where the effect of the anesthesia on withdraw reflex was tested.

The experiment was conducted according to the following protocol:

- Session 1 Protocol: Acquire a baseline discomfort threshold in an awake previously unanesthetized rat in a hot water bath experiment before any neural stimulation therapy.

- Session 2 Protocol: Acquire a baseline discomfort threshold in a rat previously anesthetized for a total duration for 10 minutes with 1.5% isoflurane and then immediately retest after activity regain.

- Session 3 Protocol: Acquire a experimental discomfort threshold of the rat after a 10 min 1.5% anesthetization during which ultrasound was applied for neural stimulation. The ultrasound was applied during the entire 10 minutes of anesthetization.
    - Therapy A: 800us pulses at 4 Hz for 10 min at 75% threshold where threshold was the minimum intensity which evoked muscle twitch.
    - Therapy B: 300us pulses at 4 Hz for 10 min at 170% threshold where threshold was the minimum intensity which evoked muscle twitch.

Session 1 Result:

The trials were conducted every 5 min. And the leg with the stimulator of the rat was soaked into the water bath when the water is heated up to 30 degree centigrade.

Trial Number	Starting Temperature (Degree Centigrade)	Withdraw Temperature (Degree Centigrade)
1	30	44
2	30	44
3	30	43
4	30	44
5	30	45
6	30	44
7	30	46
8	30	46
9	30	46
10	30	45
11	30	44
12	30	45
13	30	47
14	30	45
15	30	44
16	30	43
17	30	45
18	30	44
19	30	44
20	30	41
21	30	45
22	30	46
23	30	45
24	30	44
25	30	45
26	30	46
27	30	42
28	30	44
29	30	46
30	30	44
31	30	42
32	30	44
34	30	43
35	30	44
36	30	43
37	30	41

Table 5 Post-Surgery Baseline Discomfort Threshold
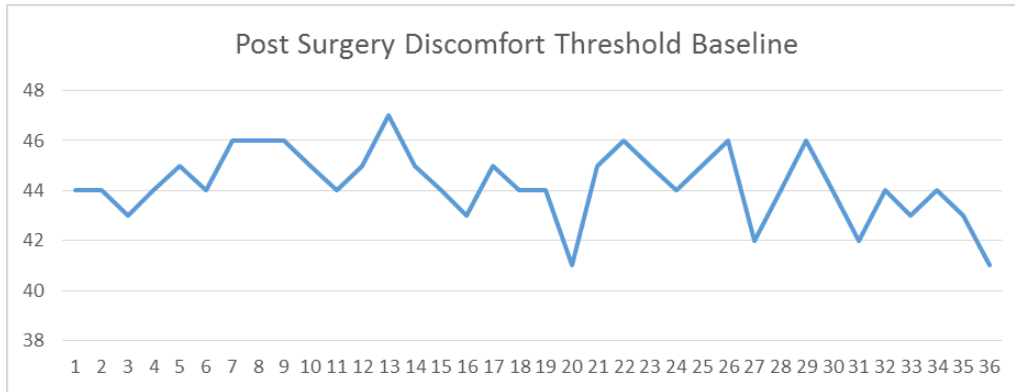
Figure 47 Post Surgery Discomfort Threshold Baseline

Session 2 Result:

After the first session of the experiment, the rat was returned to its living quarter and rested for half an hour. The rat was anesthetized using 1.5% isoflurane for 10 min, the anesthetization respirator was then removed and the rat was returned to its living quarter. After the rat was fully awake (approximately 5 min after the anesthetization respirator was removed), the hot water bath experiments were conducted.   The trials were conducted every 5 min.

Trial Number	Starting Temperature (Degree Centigrade)	Withdraw Temperature (Degree Centigrade)
1	30	42
2	30	44
3	30	45
4	30	44
5	30	42
6	30	46
7	30	46
8	30	45

Table 6 Post anesthetization discomfort threshold
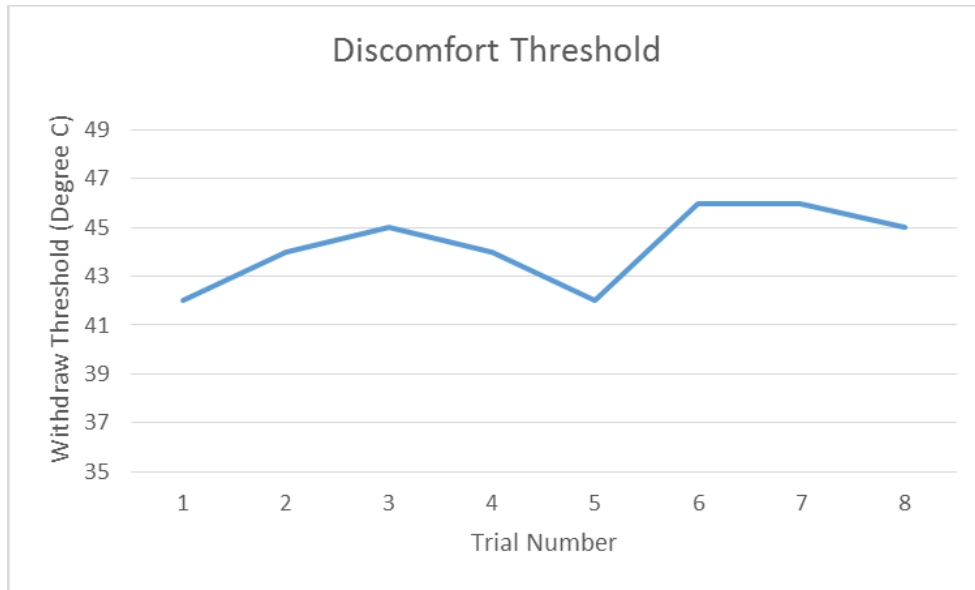
Figure 48 Post Anesthesia Discomfort Threshold Baseline

The result comparing session 1 and session 2 suggest that the effect of short duration (10 min) anesthesia is relatively little on the discomfort threshold temperature. However this is not a firm conclusion because of the relative few experiments trials that precluded the use of strong statistics analysis.   The experiment proceeded to treat the rat with the neural stimulation for 10 min with anesthesia where otherwise the rat will be uncooperative with the therapy.

Session 3 Result

Trial Number	Starting Temperature (Degree Centigrade)	Withdraw Temperature (Degree Centigrade)
1	30	36
2	30	37
3	30	38
4	30	42
5	30	37
6	30	39
7	30	38
8	30	41

Table 7 Discomfort threshold after therapy A
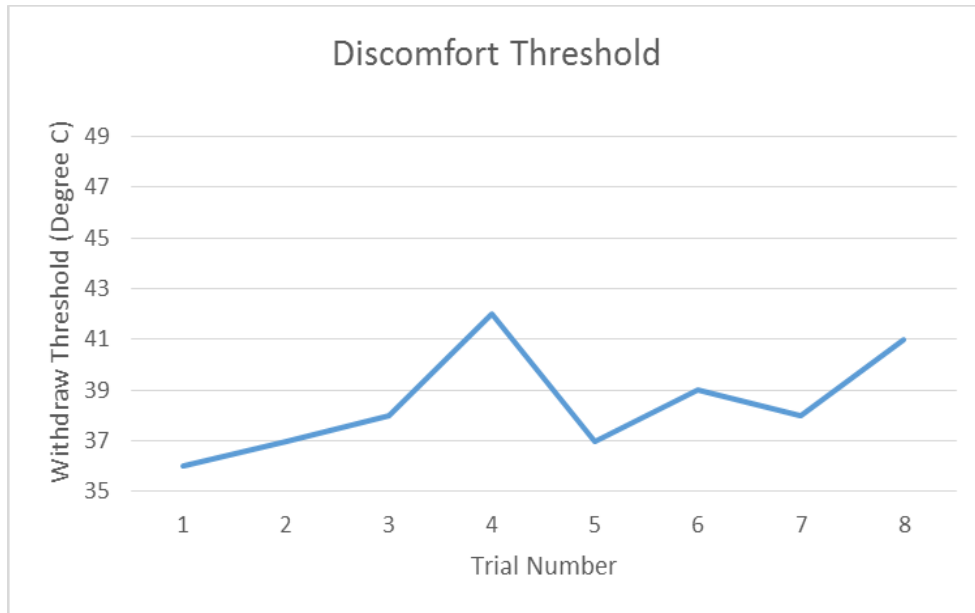
Figure 49 Post Therapy A Discomfort Threshold

As we can see from table 7 and Figure 49, the discomfort threshold was decreased substantially 4-6 degrees centigrade. This unexpectedly suggested that this type of stimulation therapy cause the increase of the pain perception. Again due to the limited data in this trial, the result could not be confirmed, but as a result, a different stimulation pulse protocol was used for another trial.

Trial Number	Starting Temperature (Degree Centigrade)	Withdraw Temperature (Degree Centigrade)
1	30	46
2	30	45
3	30	42
4	30	41
5	30	43
6	30	44
7	30	45
8	30	46

Table 8 Discomfort threshold after therapy B
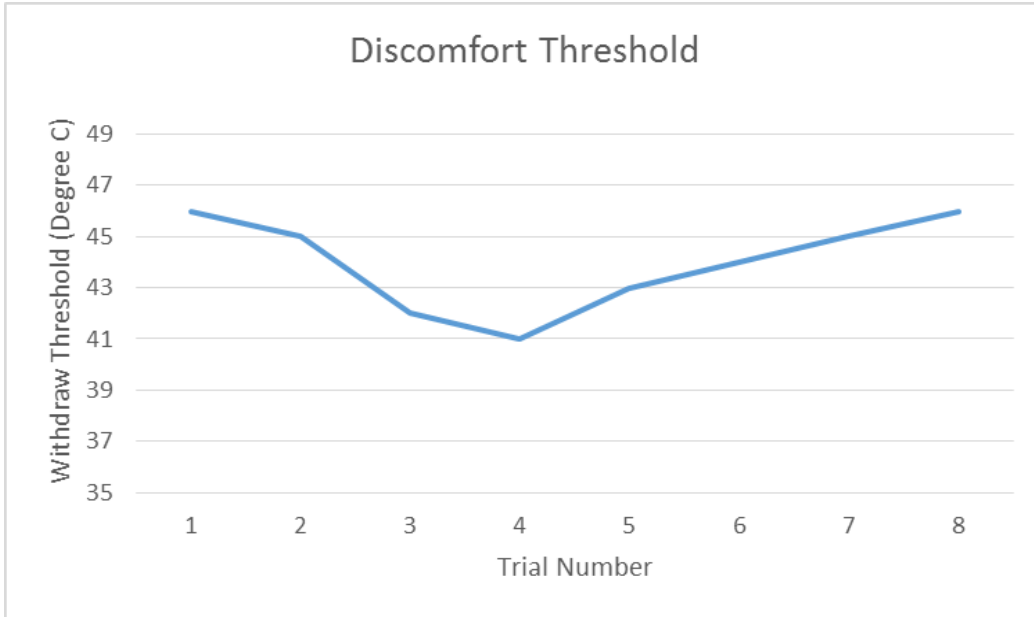
Figure 50 Post Therapy B Discomfort Threshold

On another day, and as part of the protocol of Session 3 therapeutic B protocol was employed using a higher stimulation current, the result can be seen in table 8 and Figure 50. In this experiment, the discomfort threshold was in the same range as the baseline. So unlike the prior experiment of Therapy A protocol, this trial did not support the earlier observation and appeared to show little therapeutic effect. To what extent this could be attributed to the anesthesia is unclear due to the limited data set.
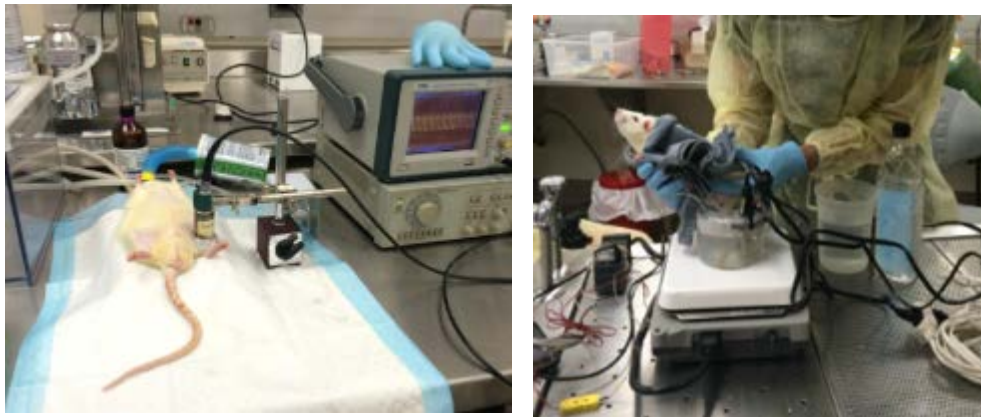
Figure 51 Ultrasound Therapy and Discomfort Threshold Measuring

CHAPTER 5

DISCUSSION

This work has investigated the design, construction and tested the performance of an implantable neural stimulator design on a pain reduction model on a rat. The piezoelectric device show sufficient current output to stimulate the sciatic nerve in a living rat and we investigated in their angular dependence.

The experiment shows both mathematically using a model as well as experimentally, the problem of achieving consistent performance with ultrasound transducers applied to the implanted devices with varying orientation as might be expected in clinical use. This high sensitivity to angular orientation is a significant problem that must be overcome for any ultrasound powered neural stimulation medical technology.

This resulted in a variation of generated current by the implant that suggested, by observing muscle twitching, was a large uncertainty when the device was employed in a lower power therapeutic mode where twitching did not occurred. This clearly attributes to experimental uncertainty regarding the therapeutic trials.

- To alleviate the angular sensitivity, a numbers of approaches were considered:
- Decrease the size of the devices.
- Reduce the frequency of the ultrasound.
- Implant multiple devices.

The study suggested that an different animal model required to assessing the neural stimulation for pain relief. Anesthesia is undesirable as a way of sedating rat or making them immobile while the ultrasound is applied to the skin. However few other methods were considered as alternative to the anesthesia. A few weeks of training to the rat did not accommodate him sufficiently to be tame so that the ultrasound can be applied while awake.

The studies of the pain relief effect involved much time and effort to accommodate the rat. And there were clearly different temperaments in different rats where only certain rats were tame enough to perform the foot withdraw test.

59

The hot water bath experimental approach relies too much on the selection and temperaments of the rats. It is desirable to have an experimental set up that does not require anesthesia and can work with living rats which do not have to be accommodated by handling and still give consistent indication of discomfort threshold.

CHAPTER 6

CONCLUSION

This work has evaluated the performance of a neural stimulator integrated with a piezoelectric component and powered by ultrasound for the purpose of pain relief in PVD. The principle results of the study showed the high dependence of the device on the incident ultrasound application angle that caused a strong change on the implant output with transducer position. Computer models verified the high sensitivity to angular incident and suggest that using smaller piece of PZT is a way to improve the performance of the device.

The devices constructed in this study are much smaller than those which have been reported in the past, and experiments showed their abilities to effectively perform neural stimulation.

In-vivo experiments in animal model demonstrated the devices' functionality in neural stimulation, although further experiments are needed to seek effective stimulation patterns for pain management. The animal experiments showed a modulation of the discomfort threshold in the rat due to the neural stimulator.

Future studies need to focus on the improvement of the in-vivo experimental model so that anesthesia is not required to immobilize the animal during the ultrasound application to the skin.

REFERENCES

[1]   "Peripheral Arterial Disease (PAD) Fact Sheet." Centers for Disease Control and Prevention. (2011) http://www.cdc.gov/dhdsp/data_statistics/fact_sheets/fs_pad.htm

[2]   Jensen, Jack E., et al. "The use of transcutaneous neural stimulation and isokinetic testing in arthroscopic knee surgery." The American journal of sports medicine 13.1 (1985): 27-33.

[3]   Galvani, Luigi (1737C1798)". Eric Weisstein's World of Scientific Biography. Wolfram Research.

[4]   Slavin, Konstantin V. "Peripheral nerve stimulation for neuropathic pain." Neurotherapeutics 5.1 (2008): 100-106.

[5]   Freudenrich, Ph.D., Craig. "How Pain Works" 09 November 2007. HowStuffWorks.com. <http://science.howstuffworks.com/life/inside-the-mind/human-brain/pain.htm>   22 October 2014.

[6]   Melzack, Ronald, and Patrick D. Wall. "Pain mechanisms: a new theory." Survey of Anesthesiology 11.2 (1967): 89-90.

[7]   Romita, V. V., and J. L. Henry. "Intense peripheral electrical stimulation differentially inhibits tail vs. limb withdrawal reflexes in the rat." Brain research 720.1 (1996): 45-53.

[8]   Towe, Bruce C. "Passive backscatter biotelemetry for neural interfacing." Neural Engineering, 2007. CNE'07. 3rd International IEEE/EMBS Conference on. IEEE, 2007.

[9]   Ozeri, Shaul, and Doron Shmilovitz. "Ultrasonic transcutaneous energy transfer for powering implanted devices." Ultrasonics 50.6 (2010): 556-566.

[10]   Arra, Satu, et al. "Ultrasonic power and data link for wireless implantable applications." Wireless Pervasive Computing, 2007. ISWPC'07. 2nd International Symposium on. IEEE, 2007.

[11]   Phillips, W. B., B. C. Towe, and P. J. Larson. "An ultrasonically-driven piezoelectric neural stimulator." Engineering in Medicine and Biology Society, 2003. Proceedings of the 25th Annual International Conference of the IEEE. Vol. 2. IEEE, 2003.

[12]   Kawanabe, Hideyuki, et al. "Power and information transmission to implanted medical device using ultrasonic." Japanese journal of applied physics 40.5S (2001): 3865.

[13]   Shih, Wen-Pin, and Wen-Pin Shih. "Design, fabrication, and application of bio-implantable acoustic power transmission." Microelectromechanical Systems, Journal of 19.3 (2010): 494-502.

[14]   Larson, Patrick J., and Bruce C. Towe. "Miniature ultrasonically powered wireless nerve cuff stimulator." Neural Engineering (NER), 2011 5th International IEEE/EMBS Conference on. IEEE, 2011.

[15]   Uchino, Kenji. Introduction to piezoelectric actuators and transducers. PENNSYLVANIA STATE UNIV UNIVERSITY PARK, 2003.

[16]   Piezo System, Inc. "Introduction To Piezoelectricity"

[18]   "Interfacing Piezo Film to Electronics."   Measurement Specialties. March 2006. Retrieved December 2, 2007.

[19]   Vázquez Carazo, Alfredo. "Novel piezoelectric transducers for high voltage measurements." (2000).

[20]   Bölcskei, Kata, et al. "Heat injury-induced drop of the noxious heat threshold measured with an increasing-temperature water bath: a novel rat thermal hyperalgesia model." European journal of pharmacology 564.1 (2007): 80-87.

APPENDIX A

MATLAB CODE

```matlab
function varargout = pzt(varargin)
% PZT MATLAB code for pzt.fig
%      PZT, by itself, creates a new PZT or raises the existing
%      singleton*.
%
%      H = PZT returns the handle to a new PZT or the handle to
%      the existing singleton*.
%
%       PZT('CALLBACK',hObject,eventData,handles,...) calls
the local
%      function named CALLBACK in PZT.M with the given input
arguments.
%
%      PZT('Property','Value',...) creates a new PZT or raises
the
%      existing singleton*.  Starting from the left, property
value pairs are
%      applied to the GUI before pzt_OpeningFcn gets called.  An
%       unrecognized property name or invalid value makes
property application
%       stop.  All inputs are passed to pzt_OpeningFcn via
varargin.
%
%       *See GUI Options on GUIDE's Tools menu.  Choose "GUI
allows only one
%      instance to run (singleton)".
%
% See also: GUIDE, GUIDATA, GUIHANDLES

% Edit the above text to modify the response to help pzt

% Last Modified by GUIDE v2.5 17-Mar-2014 19:56:53

% Begin initialization code - DO NOT EDIT
gui_Singleton = 1;
gui_State = struct('gui_Name',       mfilename, ...
                   'gui_Singleton',  gui_Singleton, ...
                   'gui_OpeningFcn', @pzt_OpeningFcn, ...
                   'gui_OutputFcn',  @pzt_OutputFcn, ...
                   'gui_LayoutFcn',  [] , ...
                   'gui_Callback',   []);
if nargin && ischar(varargin{1})
   gui_State.gui_Callback = str2func(varargin{1});
```

```matlab
end

if nargout
    [varargout{1:nargout}]     =     gui_mainfcn(gui_State,
varargin{:});
else
    gui_mainfcn(gui_State, varargin{:});
end
% End initialization code - DO NOT EDIT


% --- Executes just before pzt is made visible.
function pzt_OpeningFcn(hObject, eventdata, handles, varargin)
% This function has no output args, see OutputFcn.
% hObject    handle to figure
% eventdata  reserved - to be defined in a future version of
MATLAB
% handles    structure with handles and user data (see GUIDATA)
% varargin   command line arguments to pzt (see VARARGIN)

% Read in image
PZTpic =imread('pic.png');
% Switch active axes to the one you made for the image.
axes(handles.axes3);
% Put the image array into the axes so it will appear on the
GUI
imshow(PZTpic);


% Choose default command line output for pzt
handles.output = hObject;

% Update handles structure
guidata(hObject, handles);

% UIWAIT makes pzt wait for user response (see UIRESUME)
% uiwait(handles.figure1);


% --- Outputs from this function are returned to the command
line.
function  varargout  =  pzt_OutputFcn(hObject,  eventdata,
handles)
```

```matlab
% varargout   cell array for returning output args (see
VARARGOUT);
% hObject    handle to figure
% eventdata  reserved - to be defined in a future version of
MATLAB
% handles    structure with handles and user data (see GUIDATA)

% Get default command line output from handles structure
varargout{1} = handles.output;




function edit1_Callback(hObject, eventdata, handles)
% hObject    handle to edit1 (see GCBO)
% eventdata  reserved - to be defined in a future version of
MATLAB
% handles    structure with handles and user data (see GUIDATA)
g31=str2double(get(handles.edit1,'string'))
handles.g31=g31;

handles.output = hObject;
% Update handles structure
guidata(hObject, handles);
% editboxname is the tag of the edit box.

% Hints: get(hObject,'String') returns contents of edit1 as text
%        str2double(get(hObject,'String')) returns contents of
edit1 as a double




% --- Executes during object creation, after setting all
properties.
function edit1_CreateFcn(hObject, eventdata, handles)
% hObject    handle to edit1 (see GCBO)
% eventdata  reserved - to be defined in a future version of
MATLAB
% handles    empty - handles not created until after all
CreateFcns called

% Hint: edit controls usually have a white background on Windows.
%       See ISPC and COMPUTER.
if    ispc    &&    isequal(get(hObject,'BackgroundColor'),
get(0,'defaultUicontrolBackgroundColor'))
```

```matlab
    set(hObject,'BackgroundColor','white');
end




function edit2_Callback(hObject, eventdata, handles)
% hObject    handle to edit2 (see GCBO)
% eventdata  reserved - to be defined in a future version of
MATLAB
% handles    structure with handles and user data (see GUIDATA)
g33=str2double(get(handles.edit2,'string'))
handles.g33=g33;

handles.output = hObject;
% Update handles structure
guidata(hObject, handles);
% Hints: get(hObject,'String') returns contents of edit2 as text
%        str2double(get(hObject,'String')) returns contents of
edit2 as a double


% --- Executes during object creation, after setting all
properties.
function edit2_CreateFcn(hObject, eventdata, handles)
% hObject    handle to edit2 (see GCBO)
% eventdata  reserved - to be defined in a future version of
MATLAB
% handles    empty - handles not created until after all
CreateFcns called

% Hint: edit controls usually have a white background on Windows.
%       See ISPC and COMPUTER.
if    ispc    &&    isequal(get(hObject,'BackgroundColor'),
get(0,'defaultUicontrolBackgroundColor'))
    set(hObject,'BackgroundColor','white');
end




function edit4_Callback(hObject, eventdata, handles)
% hObject    handle to edit4 (see GCBO)
% eventdata  reserved - to be defined in a future version of
MATLAB
```

```matlab
% handles    structure with handles and user data (see GUIDATA)
length=str2double(get(handles.edit4,'string'))
handles.length=length;

handles.output = hObject;
% Update handles structure
guidata(hObject, handles);
% Hints: get(hObject,'String') returns contents of edit4 as text
%        str2double(get(hObject,'String')) returns contents of
edit4 as a double


% --- Executes during object creation, after setting all
properties.
function edit4_CreateFcn(hObject, eventdata, handles)
% hObject    handle to edit4 (see GCBO)
% eventdata  reserved - to be defined in a future version of
MATLAB
% handles    empty - handles not created until after all
CreateFcns called

% Hint: edit controls usually have a white background on Windows.
%       See ISPC and COMPUTER.
if    ispc    &&    isequal(get(hObject,'BackgroundColor'),
get(0,'defaultUicontrolBackgroundColor'))
    set(hObject,'BackgroundColor','white');
end



function edit5_Callback(hObject, eventdata, handles)
% hObject    handle to edit5 (see GCBO)
% eventdata  reserved - to be defined in a future version of
MATLAB
% handles    structure with handles and user data (see GUIDATA)
thickness=str2double(get(handles.edit5,'string'))
handles.thickness=thickness;

handles.output = hObject;
% Update handles structure
guidata(hObject, handles);
% Hints: get(hObject,'String') returns contents of edit5 as text
%        str2double(get(hObject,'String')) returns contents of
```

```matlab
    edit5 as a double



% --- Executes during object creation, after setting all
properties.
function edit5_CreateFcn(hObject, eventdata, handles)
% hObject    handle to edit5 (see GCBO)
% eventdata  reserved - to be defined in a future version of
MATLAB
% handles    empty - handles not created until after all
CreateFcns called

% Hint: edit controls usually have a white background on Windows.
%       See ISPC and COMPUTER.
if    ispc    &&    isequal(get(hObject,'BackgroundColor'),
get(0,'defaultUicontrolBackgroundColor'))
    set(hObject,'BackgroundColor','white');
end




function edit6_Callback(hObject, eventdata, handles)
% hObject    handle to edit6 (see GCBO)
% eventdata  reserved - to be defined in a future version of
MATLAB
% handles    structure with handles and user data (see GUIDATA)
width=str2double(get(handles.edit6,'string'))
handles.width=width;

handles.output = hObject;
% Update handles structure
guidata(hObject, handles);
% Hints: get(hObject,'String') returns contents of edit6 as text
%        str2double(get(hObject,'String')) returns contents of
edit6 as a double


% --- Executes during object creation, after setting all
properties.
function edit6_CreateFcn(hObject, eventdata, handles)
% hObject    handle to edit6 (see GCBO)
% eventdata  reserved - to be defined in a future version of
MATLAB
```

```matlab
% handles    empty - handles not created until after all
CreateFcns called

% Hint: edit controls usually have a white background on Windows.
%       See ISPC and COMPUTER.
if    ispc    &&    isequal(get(hObject,'BackgroundColor'),
get(0,'defaultUicontrolBackgroundColor'))
    set(hObject,'BackgroundColor','white');
end




function edit7_Callback(hObject, eventdata, handles)
% hObject    handle to edit7 (see GCBO)
% eventdata  reserved - to be defined in a future version of
MATLAB
% handles    structure with handles and user data (see GUIDATA)
frequency=str2double(get(handles.edit7,'string'))
handles.frequency=frequency;

handles.output = hObject;
% Update handles structure
guidata(hObject, handles);
% Hints: get(hObject,'String') returns contents of edit7 as text
%        str2double(get(hObject,'String')) returns contents of
edit7 as a double




% --- Executes during object creation, after setting all
properties.
function edit7_CreateFcn(hObject, eventdata, handles)
% hObject    handle to edit7 (see GCBO)
% eventdata  reserved - to be defined in a future version of
MATLAB
% handles    empty - handles not created until after all
CreateFcns called

% Hint: edit controls usually have a white background on Windows.
%       See ISPC and COMPUTER.
if    ispc    &&    isequal(get(hObject,'BackgroundColor'),
get(0,'defaultUicontrolBackgroundColor'))
    set(hObject,'BackgroundColor','white');
end
```

```matlab
% --- Executes on button press in pushbutton1.
function pushbutton1_Callback(hObject, eventdata, handles)
UpdateAxis(handles);
% hObject    handle to pushbutton1 (see GCBO)
% eventdata  reserved - to be defined in a future version of
MATLAB
% handles    structure with handles and user data (see GUIDATA)

function UpdateAxis(handles)
theta=(handles.shift)*pi/180:0.05*pi:3*pi;
vlong=handles.g33*abs(cos(theta))+handles.g31*abs(sin(theta
))*handles.thickness/handles.width
axes(handles.axes4)
plot(theta*180/pi-handles.shift,abs(vlong),'b');
xlabel('degree')
ylabel('normalized output')
hold on


function Update2(handles)
f=handles.frequency; % frequency
lambda=1570/f;
halflmd=lambda/2;
l=handles.length; % length
pp=(handles.shift)*pi/180:0.01:3*pi;
ii=zeros(size(pp));
i=1;
%%the transverse effect is about 10% of the longitudinal effect,
we ignore
%%it here
for theata=(handles.shift)*pi/180:0.01:3*pi;
lw=abs(l*cos(theata)); %total effective length
lc=abs(l*sin(theata)); %total length related to cancelation
eff=1;
if lc>halflmd
    m=floor(lc/halflmd);
    if mod(m, 2) == 0 %even
        eff= abs((lc/halflmd-m)*halflmd/lc);  %a  fraction  of
(halfwave/lc)
    else  %odd
        eff= abs((1-(lc/halflmd-m))*halflmd/lc);
```

```matlab
    end
else
    eff=1;
end
output=eff*lw/l;
ii(1,i)=output;
i=i+1;



end
axes(handles.axes5)
plot(pp*180/pi-handles.shift,ii(1,:))
xlabel('degree')
ylabel('normalized output')
ii
hold on

% --- Executes on button press in pushbutton2.
function pushbutton2_Callback(hObject, eventdata, handles)
Update2(handles);
% hObject    handle to pushbutton2 (see GCBO)
% eventdata  reserved - to be defined in a future version of
MATLAB
% handles    structure with handles and user data (see GUIDATA)


% --- Executes on button press in pushbutton4.
function pushbutton4_Callback(hObject, eventdata, handles)
axes(handles.axes5)
cla;
% hObject    handle to pushbutton4 (see GCBO)
% eventdata  reserved - to be defined in a future version of
MATLAB
% handles    structure with handles and user data (see GUIDATA)


% --- Executes on button press in pushbutton3.
function pushbutton3_Callback(hObject, eventdata, handles)
axes(handles.axes4)
cla;
% hObject    handle to pushbutton3 (see GCBO)
% eventdata  reserved - to be defined in a future version of
MATLAB
```

```matlab
% handles    structure with handles and user data (see GUIDATA)



function edit8_Callback(hObject, eventdata, handles)
shift=str2double(get(handles.edit8,'string'))
handles.shift=shift;
handles.output = hObject;
% Update handles structure
guidata(hObject, handles);
% hObject    handle to edit8 (see GCBO)
% eventdata  reserved - to be defined in a future version of
MATLAB
% handles    structure with handles and user data (see GUIDATA)

% Hints: get(hObject,'String') returns contents of edit8 as text
%        str2double(get(hObject,'String')) returns contents of
edit8 as a double



% --- Executes during object creation, after setting all
properties.
function edit8_CreateFcn(hObject, eventdata, handles)
% hObject    handle to edit8 (see GCBO)
% eventdata  reserved - to be defined in a future version of
MATLAB
% handles    empty - handles not created until after all
CreateFcns called

% Hint: edit controls usually have a white background on Windows.
%        See ISPC and COMPUTER.
```

APPENDIX B

INJECTION SURGERY

The animal used was a Sprague-Dawley rat weighing 800g.

The rat was first anesthetized by inhaling 2% isoflurane, following by removal of its fur on its left hindlimb. After sterilization, a 18 gauge syringe needle capped with a catheter was introduced into the gap between the gastrocnemius and lateralis toward the sciatic nerve branch, the needle was then taken out, leaving the catheter in the tissue. A wire connected with a pulse generator was introduced into the catheter carrying a 10V 100ms stimulation pulse. This was to identify twitching of the rat's high limb in order to find the proper implantation site. As Figure 52 shows.

Figure 52 The Injection Procedure

At the position identified by the twitching, a device was advanced through the catheter with its cathode pointing toward the nerve, the catheter was then flushed with saline so it pushed the device into the tissue at the desired implantation site.

Ultrasound was then applied to the rat's hind limb in order to confirm by twitching that the implantation was right in place. This experiment failed for reasons unknown perhaps related to the placement method to evoke muscle twitching was followed by another successful experiment using surgical implantation devices.